An Investigation of Constraints on Dark Matter Models from Mono-jet Searches at LHC

Dissertation
zur
Erlangung des Doktorgrades (Dr. rer. nat.)
der
Mathematisch-Naturwissenschaftlichen Fakultät
der
Rheinischen Friedrich-Wilhelms-Universität Bonn

von
Swasti Belwal
aus
Dehradun, Indien

Bonn, October 2017

Dieser Forschungsbericht wurde als Dissertation von der Mathematisch-Naturwissenschaftlichen Fakultät der Universität Bonn angenommen und ist auf dem Hochschulschriftenserver der ULB Bonn `http://hss.ulb.uni-bonn.de/diss_online` elektronisch publiziert.

1. Gutachter:	Prof. Dr. Manuel Drees
2. Gutachter:	Prof. Dr. Herbi Dreiner

Tag der Promotion:	16.04.2018
Erscheinungsjahr:	2018

Abstract

In this work we investigate the Weakly Interacting Massive Particle (WIMP) dark matter searches in colliders. We focus on the mono-jet searches and derive the upper bounds on the WIMP production cross-sections at the LHC. Using the derived bounds we further constrain the models describing WIMP dark matter. We start by using Effective Field Theory (EFT) for our analysis. In our context, EFT for WIMP dark matter is an extension of the Standard Model by a dimension–6 operator which has a coefficient $1/\Lambda^2$, where Λ is the regulating scale upto which the effective theory analysis is safely applicable. We do the analysis for both the 8 TeV and 13 TeV searches at the ATLAS and CMS experiments of LHC. We also combine the 8 TeV data of ATLAS and CMS collaborations and observe that this approach improves the individual bounds only very little.

The EFT is able to accurately describe the contributions from the $\mathcal{O}(\Lambda^{-2})$ to the tree-level matrix element. However, we show that the tree level matrix element receives significant contributions of order Λ^{-4} for the values of Λ near the current bound. When these higher order contributions of Λ are considered they strengthen the current upper bounds on the WIMP cross-section significantly. In case of a simplified model, such contributions further correspond to the processes where two mediators are exchanged. EFT interpretations face difficulties when the higher order operators, like dimension–8 operators, are not taken into consideration. The Λ^{-4} contributions to the matrix element from a double mediator exchange are similar to the $\mathcal{O}(\Lambda^{-4})$ contributions coming from the dimension–8 operators. Based on our observations, we challenge the internal consistency of the EFT description.

We further translate the bounds obtained from the effective theory to the simplified models. We study the mono-jet signals for the $s-$channel mediator in the simplified model where the mediator's width can be accurately calculated. We then show that if the mediator's width is small then the simplified models can be accurately derived from the effective field theory only when the mediator has a mass greater than 5 TeV. This requires that the upper bounds on the cross-sections to be 16 times stronger than the current bounds at LHC. This is very unlikely for the considered parameters and hence, such a model cannot be described accurately by EFT. This application is even more redundant if the bounds at 13 TeV are to be considered. In the end we show that the inconsistency of the EFT description further makes it difficult to apply its model independent results to a well-defined model, in any sensible way.

Acknowledgements

I begin by expressing my sincere gratitude to Prof. Manuel Drees for his supervision throughout my Ph.D.. I would like to thank him for encouraging my research and for accepting me as a part of his group. I appreciate his trust and faith in my abilities and his support throughout the time which I took to develop the necessary skills needed for this work. I am thankful for his understanding and acknowledgement of the efforts required on my part. I am grateful to him for providing me the extra time to dedicate towards my Ph.D. and the financial support needed towards the end.

I am grateful to Deutscher Akademischer Austausch Dienst (DAAD) for granting me the scholarship and offering me the opportunity to work at the University of Bonn. This opportunity of experiencing the German and European culture has shaped my career and personalities to the best. I must thank Prof. Herbi Dreiner for his acceptance to be my second referee. I also thank to Prof. Ian Brock and Prof. Clemens Simmer for their keen interests in my work and for agreeing to be the third and fourth referees in my Ph.D. committee.

I am thankful to Jong for supporting me through the technical issues of my work and for all his suggestions. I am obliged to Manimala and Nicholas for spending their precious time to proof read my thesis and for offering me the much needed feedback. I can never forget to thank all the amicable BCTP members and my dear colleagues for the good times and valuable discussions.

I am deeply thankful to our secretaries, Mrs. Petra Weiss, Mrs. Patricia Zuendorf, Mrs. Christa Boersch, Mrs. Dagmar Fassbender (retd.), and our IT expert, Mr. Andreas Wisskirchen, for their very kind words and the constant support they provided. I am grateful for their efforts they put to go beyond the requirements to help me through all kinds of personal and legal matters.

I am filled with gratitude towards my life partner, Harshit, for bearing it all with me; to my sister, Shubhi, for being my rock through desperate times; and to all my friends for helping me through various stages of my stay in Bonn.

Finally, I dedicate all my honours to my parents, to whom I owe everything.

Contents

1 Introduction **1**

2 Dark Matter **5**
- 2.1 Evidences 5
- 2.2 Candidates 6
- 2.3 Searches 7

3 Effective Field Theory **11**
- 3.1 Effective theory for WIMPs 12
- 3.2 Derivation of EFT operators from a full theory 13
  - 3.2.1 Pseudo-scalar operator 14
  - 3.2.2 Axial-vector operator 18

4 Methodology **21**
- 4.1 Analysis 22
  - 4.1.1 Implementation of CMS 8 TeV analysis 24
  - 4.1.2 Implementation of ATLAS 8 TeV analysis 25
  - 4.1.3 Implementation of ATLAS 13 TeV analysis 26
- 4.2 A Combined Analysis 30

5 Inconsistency of EFT Description **31**
- 5.1 Axial-vector case 32
- 5.2 Pseudo-scalar case 36

6 A Simplified Model from EFT **39**
- 6.1 Model descriptions 39
- 6.2 Finite Width Effects and Applicability of the EFT 40
- 6.3 Implications of the EFT inconsistency 44

7 Conclusion **47**

A Appendix **57**
- A.1 Decay width of axial-vector mediator 57
  - A.1.1 Matrix element for axial-vector mediator 59
  - A.1.2 Calculation of phase-space factor 60

List of Figures **63**

List of Tables **65**

CHAPTER 1

Introduction

Our Universe has always been an element of wonder and surprises. The scientifically driven understanding of the Universe and its creation hold the key to the development and growth of mankind. Though it seems impossible to completely understand if our universe is all chaos or a magnificent crafted design, all the means have been exploited to understand our origin. The Big Bang Theory [1] appeals as a sensible explanation of our currently expanding Universe. The particles created during the Big Bang have undergone several modifications and form the large-scale structures of Universe as observed today.

For a long time the Universe was known to consist of only the visible or baryonic matter. It was in early 1930's when Jeans [2] and Oort [3] studied the random motion of the stars in the Milky Way disk. Their observations indicated towards the presence of 'extra' gravitational force responsible for such peculiar motions. Since then, numerous observations supported the presence of invisible 'Dark Matter' in the Universe and held it responsible for these gravitational anomalies. Despite its existence being observed for decades now, we know very little about the dark sector component of our Universe. Numerous observations have ruled out the massive baryonic objects to satisfy the observed abundance of dark matter in the universe, thus forcing it to be a more fundamental issue. Cosmologists aim to solve the dark matter mystery by reforming the gravitation theories to explain the missing masses in the large-scale structures. However, particle nature of the dark matter appears a more attractive solution.

If dark matter components are fundamental particles, they need to fit in a theory that is in accord with the Standard Model (SM) [4]. Dark matter cannot be a SM particle or a composite, else we would have been able to find some signature with our current experimental reach. As the nature of dark matter cannot be fully explained by the known fundamental particles, it is certain that particle dark matter needs a Beyond Standard Model (BSM) theory, and even new particles to explain its relic abundance. Several particles have been proposed, like axions and Weakly Interacting Massive Particles (WIMPs), coming from SM extensions. WIMPs have masses of the order of 1 GeV to few TeV and can couple to the SM particles through very weak interactions. In fact, with their masses of about electro-weak scale, they are the most promising candidates for dark matter as they closely satisfy the measured relic density of dark matter i.e.

$\Omega_{DM}h^2 = 0.1186 \pm 0.0020$ [5]. WIMPs could very likely be a fundamental particle and can be produced in high energy collisions. Being stable and long-lived in the collider time scales, electrically neutral, and also lacking any strong interaction, WIMPs escape any possible detection. The only way to observe a WIMP pair escaping the detection is to tag them with an associated high transverse momentum (p_T) object, like a mono-jet.

Several models based on Supersymmetry [6, 7] (e.g. Minimal Supersymmetric Standard Model(MSSM) [8]) have been proposed which naturally contain dark matter candidates. So far no signal has been observed in any dark matter experiment which could be explained by such theories. As there has been no sign of new fundamental particles in the experiments, it has become difficult to validate any BSM theory. In light of this uncertainty for the right dark matter model, it is important to have a theoretical framework which can justify the dark matter in the experiments efficiently.

Effective Field Theory (EFT) [9] comes in as a great tool to probe into the nature of dark matter. It allows us to study the possible interactions without complicating the inner physics at the interaction vertex. In EFT, the interaction between standard model and the dark matter sector is carried by a mediating particle. The mass (M) of the mediating particle is taken to be extremely large, such that it is much greater than the momentum (Q) exchanged between the interacting particles, i.e., M $\gg$ Q. With this approximation the mediator can be integrated out, leaving a four-point interaction vertex where one can easily focus on the outgoing dark matter particles with a model-independent approach. For heavy mediators, the mediating width becomes enough large that the particle-like behaviour of the mediator can be ignored. This simplifies the analysis since EFT has fewer free parameters than complete models; moreover, several models may lead to the same EFT, and can thus be treated simultaneously. Based on the mediator and WIMP properties, there are several dimensional operators for a contact interaction. In this work, we focus mainly on axial-vector and pseudo-scalar operators.

Also, ambient Dark Matter WIMPs are non-relativistic, with a mean velocity, $v \sim 10^{-3}c$. Hence, the maximal momentum exchanged in direct detection experiments is of order 100 MeV (for the scattering of a relatively heavy WIMP on a heavy target nucleus, like Xenon). Since WIMPs carry neither electric nor color charge, their interaction with quarks must be mediated by a massive particle. In most cases, the mass of this mediator is usually much larger than 100 MeV. Hence, dark matter direct detection searches can be analysed with an EFT where the mediators have been integrated out.

Mono-jet signals have also been analysed with EFT, both by theorists [10, 11], and by the Large Hadron Collider (LHC) collaborations [12, 13]. Clearly, this can be expected to accurately reproduce the results obtained in a renormalizable theory only if the momentum flow through the mediator is much smaller than the mass of this mediator. The most sensitive search region for the 8 TeV data requires missing transverse momentum of about 500 GeV. One may then conclude that the EFT description should work if the mediator mass is (well) above 500 GeV. In fact, this estimate is not that far off for $t-$channel mediators [14]. However, in this work we will see that the exchange of narrow $s-$channel mediators can be accurately modelled by an EFT only for mediator masses above 5 TeV.

The experimental bounds on the cut-off scale 'Λ'[1], upto which the EFT formulation is valid, are around 1 TeV. These bounds on the Λ can be saturated only if the mediator's couplings to quarks and/or WIMPs are considerably above 1, i.e. for strongly interacting theories. Moreover, we find that even in this case some contributions to the matrix element for WIMP production, that are of order Λ^{-4}, are sizeable. This means that an accurate EFT treatment would need to also include dimension-8 operators, thereby introducing several new parameters and thus spoiling the main advantage of EFTs. Thus, simply ignoring all these Λ^{-4} terms (which so far has been a standard practice in the experimental analyses) means that the EFT applied to mono-jet searches does not accurately describe *any* renormalizable theory with a $s-$channel mediator, if the scale Λ is near the experimental lower bound.

The chapters in this thesis are structured as follows. We begin with a brief discussion of dark matter properties, evidences and detection techniques in Chapter 2. In Chapter 3, the theoretical framework of EFT is discussed in detail and the operators used for the analysis are derived. We discuss our methodology and analyses in Chapter 4, with the focus on the collider mono-jet searches for WIMPs. We discuss our analysis for the $\sqrt{s} = 8$ TeV and 13 TeV and validate our results with current experimental bounds on the cut-off scale. We combine the experimental data from both ATLAS and CMS experiments for an improvement on their individual bounds. In Chapter 5 we discuss our key results. We show that there is an inconsistency in the EFT analysis as several contributions from tree-level sub-processes are not included. We observe that this discrepancy in the effective approach for dark matter searches makes it invalid for any precise estimations. We demonstrate that a double-mediator exchange complicates the established EFT interpretations of dark matter searches. In Chapter 6, we do a comparative study for our observations of EFT by applying them to our simplified model. We also determine the mediator mass for a realistic width in a simplified model derived from our EFT model. With our observations we explain that it is meaningless to consider a simplified model derived from such an effective theory. Finally, in Chapter 7, we conclude with a summary of our key highlights.

---

[1] Throughout this work, we depict the cut-off scale by Λ in a universal context, otherwise we add a subscript for the corresponding interaction.

CHAPTER 2

Dark Matter

The cosmological observations done by various experiments, like WMAP [15] and PLANCK [5], have well established that dark matter is stable and long-lived. From the structure formations observed by these experiments, it is required that dark matter must be non-relativistic (or *cold*) [16], as it survived the developments of our Universe. Based on the experimental observations of dark matter, we do know that:

- it has no electromagnetic interaction and is not electrically charged.
- it has no color charge and hence does not show any strong interaction.
- it may have very weak interactions, which are difficult to observe at current experiments.
- most of the dark matter evidence proves it to be massive due to its observed gravitational effects.

2.1 Evidences

Dark matter is a crucial component of our Universe. The latest cosmological data by PLANCK refines the dark energy contribution to the total energy density upto 68.3%, and dark matter contribution upto 26.8% [17]. Only the remaining 3.8% of the total energy density is contributed by the baryonic matter.

Dark Matter plays a significant role in the formation of galactic structures and clusters [18]. The discrepancies observed in the predicted galactic rotation curves, which obey Newtonian dynamics, corresponds to dark matter present in them. Based on the Kepler's law, the radial velocity of a galaxy should be $v(r) = \sqrt{GM(r)/r}$, where, G = gravitational constant and r is the distance from the galactic center. The galactic mass $M(r)$, consisting of all the visible objects and gases, is governed by the mass distribution profile of the galaxy ($\rho(r)$), such that $M(r) \equiv 4\pi \int \rho(r) r^2 dr$. This, however, does not hold for the NGC6503 galaxy as observed by Vera Rubin and collaborators in 1970's. Later, these observations were also made for several other galaxies, including Milky Way [19, 20]. The discrepancies in these curves indicate the presence of an invisible mass in the respective galaxies.

Fritz Zwicky in 1933 observed the velocity dispersion of the galaxies in Coma cluster. However, he found the Doppler shifts for the system were higher by 1000-2000 km/sec, indicating higher velocities than predicted using the Virial theorem [21]. This could have been possible only if the mass of the Coma cluster was 400 times larger than the observed luminous mass. Gravitational lensing of the Coma cluster indeed confirms such observations. Similar discoveries have been made for other galaxies with lower mass-to-light ratios. Gravitational lensing in $Abell2218$ [22] and the Bullet cluster collisions [23] stressed on the fact that the dark matter present in these clusters governs their dynamics with its strong and weak gravitational effects.

Cosmic Microwave Background (CMB) observations have revealed more valuable insights on dark matter being responsible for the large-scale structures that we observed today. The temperature fluctuation of CMB through its propagation occurring due to compression and expansion of the universe due to mass and radiation pressure, can be carefully translated into its power spectrum. As the peaks of the spectrum can give the most precise details on the matter and energy compositions of the Universe, it establishes that the dark energy and dark matter define the major contributions [5]. The baryonic acoustic oscillations (BAO), which can be observed in the CMB power spectrum further indicate on their interactions with possible dark matter along their propagation [24, 25].

Attempts to discard any dark matter being responsible for such observations have been made by modifying the gravitational theories but rather unsuccessfully. For example, Modified Newtonian Dynamics (MOND) [26] does reproduces the rotational curves of the galaxies, but fails to explain the observed matter density and the large-scale structure formation in the absence of dark matter.

2.2 Candidates

Particle nature of dark matter is so far the most promising and realistic. The baryonic dark matter has been ruled out, being insufficient to substitute the observed relic density. Non-baryonic dark matter is a more compelling possibility as dark matter has escaped detection up to now. The fact that dark matter can also be a fundamental particle has ignited theoretical reforms. It is certain that dark matter is a particle beyond the SM and needs new theories which are either an extension of the SM [27], or naturally contain SM within them (e.g. SUSY).

Sterile neutrinos as dark matter have been excluded recently [28]. Even though SM neutrinos seem to fit as dark matter candidates, they are ultra-relativistic to form the large-scale structures and hence, cannot account for the observed abundance [29]. QCD axions arising as the Pecci-Quinn solution to the strong-CP problem are one of the promising candidates for light dark matter [30]. Axions are the only SM candidates which are comfortably accommodated as dark matter. However, with their theoretical mass range of only a few eVs, they cannot suffice for dark matter relic density. Other complex particles, like Q-balls [31] and Wimpzillas [32], are too heavy and face stability issues and theoretical challenges.

WIMPs are by far the most promising dark matter due to their natural properties. They arise naturally from beyond standard model theories as exotic (non-standard) and fundamental particles, like SUSY candidates [33] (for e.g., neutralinos, sneutrinos, gravitinos and axinos), and Kaluza-Klein states coming from higher dimensional string theories [34]. Being fundamental particles, WIMPs are assumed to be the relics from the freeze-out era. They are mainly proposed to be non-thermal and fundamental such that they do not decay into SM particles.

The relic density in terms of Hubble parameter is given as,

$$\Omega_\chi h^2 \approx \frac{3 \times 10^{-27} cm^3 s^{-1}}{\langle \sigma v \rangle} \tag{2.1}$$

where, χ stands for the WIMP, and Hubble parameter $h = H_0/100\ kms^{-1}Mpc^{-1}$. $\langle \sigma v \rangle$ is the thermally averaged WIMP annihilation cross-section. The latest Planck results give the dark matter abundance of :

$$\Omega_\chi h^2 = 0.112 \pm 0.009 \tag{2.2}$$

This gives the self annihilation cross-section for WIMPs as:

$$\langle \sigma v \rangle \approx 3 \times 10^{-26} cm^3 s^{-1} \tag{2.3}$$

Thus, WIMPs have masses in the range of 10 GeV to 1 TeV which is within the range of weak interactions. In fact, particles like neutralinos have masses of order of few GeVs to satisfy the dark matter abundance and stand out as interesting WIMP candidates. This advantage of WIMPs having mass in this range, and their ability to naturally satisfy the dark matter relic density, is the so called 'WIMP miracle!'.

2.3 Searches

Concentrating mainly on the non-baryonic dark matter, the experimental searches look for new and exotic particles [35]. Dark matter searches are broadly summarized into three categories: direct searches, indirect searches and collider searches, Fig.(2.1).

Direct detection of WIMPs is one of the most promising dark matter searches. Given their high density in our galactic halo, a good number of WIMPs certainly pass through the Earth and collide with the baryonic matter. The direct detection experiments aim to detect these collisions of the WIMPs with the nuclei of a stable element by measuring the recoil energy of the nuclei. The approximate local density of WIMPs around the sun is 0.39 GeV/cm^3, and their mean velocity in the halo is about 220 km/s. From this, one can calculate the average rate of interaction for a WIMP-nucleon scattering as:

$$R \approx \sum_i N_i n_\chi \langle \sigma_{i\chi} \rangle \tag{2.4}$$

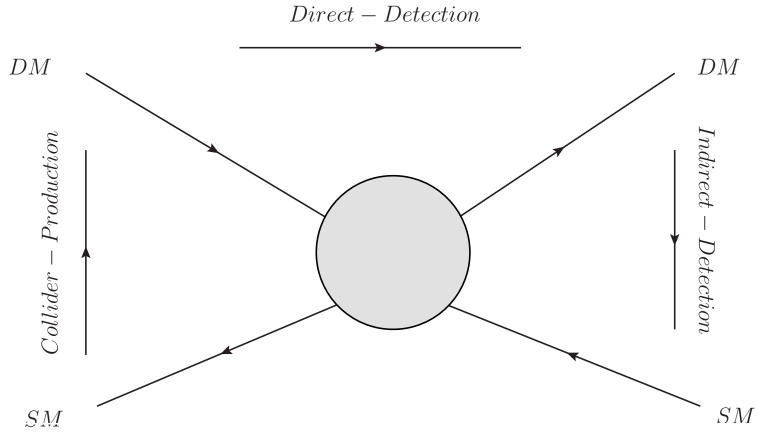

Figure 2.1: The three categories of dark matter searches related to each other with crossing symmetry. Here, DM stands for Dark Matter particles, and SM for Standard Model particles.

where, N_i is the number of nuclear species (or elements) present in the detector with i corresponding to different nuclei species, n_χ is the local WIMP density, and $\langle \sigma_{i\chi} \rangle$ is the cross-section for WIMP scattering off i^{th} species of nuclei in the detector.

The scattering cross-section can be either elastic, where phonons are recorded to generate the recoil energy spectrum of the nuclei, or in-elastic, where the nuclei are left in an excited state after the collision and are detected by a photon emitted in the event. CDMS, CRESST, XENON 100 are some example of experiments which use similar techniques of studying the WIMP-nuclear recoils [36]. Another interesting way to observe WIMPs is to study the annual solar modulation. Due to the location of the hemisphere with respect to the sun, the experiments receive different inflow of the WIMPs at different times of the year, as recorded by DAMA [37].

WIMPs could be scalars, vectors, Dirac or Majorana spinors. Based on the interaction that WIMP has with nuclei, their scattering can be spin-dependent and spin-independent. Spin-dependent scattering occurs for axial-vector, pseudo-scalar, and tensor-like interactions, and is dependent on the residual spin factor of the nuclei, i.e J(J+1). The scalar and vector interactions result in the spin-independent scatterings, and hence are more dominated in the direct detection experiments. For studying spin-independent interaction, stable nuclei with neutral spins, like Ge and Xe, are considered such that they have significantly higher masses. For spin-dependent interactions nuclei with residual spins are important, like 19F and 23Na. Direct detection can give best sensitivity for WIMP masses nearly equal to the nucleus mass to gain resonance in the recoil energy for an easily distinguishable signal. The direct detection limits the upper bounds on the cross-sections being as low as of order $10^{-45} - 10^{-46}$ cm^2 for WIMP masses in the range of 10 GeV to 1 TeV [38].

Indirect detection, as the term indicates, focuses on detecting particles or residues (referred to as 'Smoking gun' signals) arising from dark matter annihilations at ultra-high energies. Such active regions with very high energies (like the center of our galaxy) where dark matter can annihilate, have extremely high average temperature for WIMPs to be ‘hot’ enough (relativistic) and to have significant collision rates. The residual final states after WIMPs annihilating into SM particles are generally high energy γ rays or positrons, which are being looked by experiments like FermiLAT [39]. When captured inside the sun, WIMPs can annihilate into a pair of neutrinos. Hence, these localized and increased fluxes would be a good WIMP signal, as being looked upon by IceCube [40].

High energy particle colliders for long have been actively searching for new and exotic particles. This year, LHC reached the landmark of having a center of mass energy of 13 TeV, with an upcoming upgrade of 14 TeV and a promised increase in the luminosity by a factor of 10 [41]. The idea behind the collider searches is to actually produce dark matter in high-energy collisions and observe it in the detectors like ATLAS [13] and CMS [12]. As this work focuses on the current WIMP searches at the LHC, we discuss the analysis techniques and our results for mono-jet searches later in much detail.

CHAPTER 3

Effective Field Theory

In order to verify a WIMP detection, it is important to have a self-sufficient theoretical model capable of validating the WIMP signals in the experiments. Some issues which need to be targeted while building a dark matter theory are:

- The theory needs to be an extended version of the standard model. This means that at least one of the particles in the extension must have a portal to interact with the standard model particles if it is to satisfy the pre-freeze out equilibrium of WIMPs and SM particles.
- It must be renormalizable and, without any ultra-violet (UV) and self-diverging mass terms.
- The theory must be valid at the Planck scale and should not violate the hierarchy, i.e. the particles must have masses in the range to avoid any irregularities when going beyond the SM scale.
- Lastly, the theory should contain natural and fundamentally stable WIMPs which can satisfy the dark matter relic density and can explain all the dark matter evidence to a good extent.

Creating such a self-sufficient and validating theory is difficult as it requires the knowledge of a large parameter space for accurate interpretations. For example, SUSY naturally contains neutralinos (like bino and wino), which perfectly qualify to be WIMPs as they are weakly interacting and their masses can be in the range of a few GeV. In an attempt to reduce the parameter dependence on the searches minimal SUSY models, like pMSSM, has been introduced. This indeed reduces the number of independent parameters significantly but one risks losing the relevant details which might lead to misinterpretations.

To avoid such complications, one often looks into simplified models [42] with only the minimal particles, like a WIMP pair and a mediator that connects the WIMPs to the SM particles, thus reducing all the unnecessary effort of determining hundreds of parameters

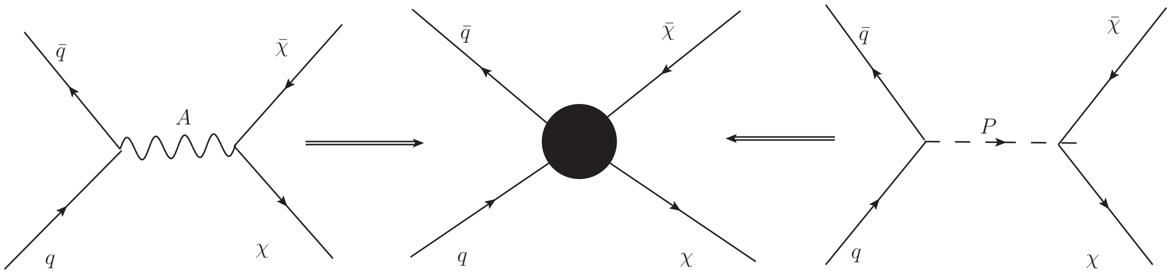

Figure 3.1: An interaction vertex is shown in the middle. The diagram conveys how a WIMP-SM interaction via an axial-vector (A) and a pseudo-scalar (P) mediator in a full theory can be understood as a four point interaction in EFT.

as in SUSY. Even though simplified models appear practically efficient, it is difficult for them to justify themselves as a complete theory [43].

A relatively simple way to focus on dark matter searches is to follow the effective approach where one has the freedom to focus on interactions requiring minimal and only the necessary parameters. The idea behind an effective interaction is the sole purpose of making the analysis easier for the observer to understand.

3.1 Effective theory for WIMPs

In Effective field theory (EFT) prescription one treats the considered process as a low energy theory being a limit of a fundamentally higher energy theory [44–46]. A huge advantage of EFT is its flexibility to span over multiple energy scales. It helps us in studying a process as a limiting effect of an underlying full theory at some higher energy such that the phase space is restricted and the high energy degrees of freedom are not accessible. In terms of EFT, SM can be considered as a low energy theory where the higher mass scales observed at the Planck scale have been integrated out, and thus, do not affect the SM processes. Fig.(3.1) shows an example of how the processes in a full theory will correspond to an EFT vertex.

The energy scale upto which an EFT is valid is called the cut-off scale, Λ. To formulate a general effective Lagrangian one only needs the relevant degrees of freedom and symmetries of the system. A quantum field theory analysis can be performed using this general Lagrangian only if the momenta Q of all the particles is much greater than Λ. After renormalization of the mass terms, the coefficients of an effective theory operator can be related to the physical observables, making them independent of Λ.

In order to simplify a complex interaction in a complete UV theory with effective interaction, we derive the effective theory operators. We integrate out the mediator from the interaction such that we only need minimal information about the mediating particle and we can focus more on the dark matter particles and their interactions with SM particles. There are several dimensional operators for such contact interactions, for example, scalar, vector, axial-vector, pseudo-scalar, tensor and several other complicated operators [47–50].

Though the operators in themselves do not hold a physical meaning, their coefficients (including Λ) can be inferred being proportional to the couplings of the particles. The physical parameters are thus dependent on Λ as it governs the nature of underlying theory. This dependence, however, is further constrained by the renormalization group invariance and perturbativity.

EFT is a bottom-to-top approach for dark matter physics, i.e., we start with a full theory Lagrangian, use effective analysis for studying dark matter interactions, and then use the results to provide more information on the dark matter interactions in a full theory. At colliders, an EFT analysis gives an upper bound on Λ, whereas the lower bounds are given by direct detection experiments [51]. This helps in focusing the WIMP searches in the regions satisfying the boundary conditions. Though an interpretation from effective analysis might not give a complete picture as all the other relevant parameters for a complete theory are not taken into account, but it indeed will help to narrow down our searches by ruling out the redundant dark matter models, and by putting limits on the parameter values.

3.2 Derivation of EFT operators from a full theory

An effective field theory (EFT) Lagrangian describing the interactions of WIMPs (χ) with SM fermions (f) can be written as [10] :

$$\mathcal{L}_{\text{EFT}} = \sum_{\Gamma} \frac{1}{\Lambda_{\Gamma}^{2}} \bar{\chi}\Gamma\chi\bar{f}\Gamma f \,. \tag{3.1}$$

Here, $\Gamma \in \{1, i\gamma_5, \gamma_\mu, \gamma_\mu\gamma_5, \sigma_{\mu\nu}\}$ for scalar, pseudo-scalar, vector, axial-vector, and tensor interactions, respectively.

To derive this EFT Lagrangian we start by taking a UV complete theory which is a simple extension of SM. We add only a fermionic WIMP pair and a mediator which regulates the interaction of the dark sector to the standard model. A general Lagrangian for WIMPs interacting with the SM particles can be given as:

$$\mathcal{L} = \mathcal{L}_{SM} + L_{WIMPs} + L_{mediator} + L_{interaction} \tag{3.2}$$

Throughout this text, we denote our WIMP dark matter with χ and consider them to be Dirac fermions to incorporate their spin-dependent interactions. Majorana fermionic WIMPs will also give similar results as Dirac fermions pertaining to their spins. The scalar WIMPs cannot interact with the considered operators in this work, and hence, are out of the context. For a simplification, we consider that our WIMPs interact only with all of the quarks (q) with an equal coupling strength, and neglect their interactions with other SM fermions like leptons. Moreover, there are stringent constraints on WIMP-lepton couplings coming from di-lepton resonance searches [52]. The motivation to make this choice is that we are focusing mainly on the collider searches for WIMPs, specifically at the proton-proton collider (LHC), where the colliding beams majorly constitute of quarks. Also, we concentrate on mono-jet searches which are relevant only for the quark interactions with WIMPs, as they require an initial state jet production.

For the EFT analysis, we consider our mediator mass to be 10 TeV. This choice of the mass ensures an off-shell production of our mediator for our both 8 TeV and 13 TeV analysis. With this we also safely avoid any resonance production of the mediator at the current LHC energies. The mass of WIMP varies in the range of 1 GeV to 1 TeV.

One of the goals of our analysis is to compare predictions derived from the EFT (eq.(3.1)) with those derived from a 'simplified model', where χ interacts with quarks via the exchange of one mediator. We focus on $s-$channel mediators for two reasons. First, $t-$channel mediators would need to carry color, whereas $s-$channel mediators do not. The latter can for e.g. be an additional gauge or Higgs bosons [53], which have been widely discussed in the literature for reasons not related to Dark Matter; such models, therefore, seem somewhat better motivated than models with $t-$channel mediators [54]. Secondly, in models with $t-$channel mediators, a Fierz transformation is required to bring the effective Lagrangian into the form of eq.(3.1) [55], which has also been used by the experimental groups. Hence, a simplified model with a $t-$channel mediator will generally produce several terms in the effective Lagrangian simultaneously, thereby complicating the analysis.

Among the $s-$channel mediators, models with a scalar (CP-even) or vector mediator will lead to spin-independent contributions to the WIMP-nucleon scattering matrix elements. Moreover, there is no renormalizable theory with mediators of spin-2, which would lead to tensor interactions. Hence, we focus on pseudo scalar (CP-odd) and axial vector mediators as:

- For the collider studies, the bounds obtained for EFT are nearly same for the vector and axial-vector operators, and similarly, for scalar and pseudo-scalar operators, as at very high energies the effects coming from spins of the particles are negligible.
- Also, spin-dependency of these operators makes them interesting for dark mater direct searches, thus allowing us to cover a wide application of our results.

3.2.1 Pseudo-scalar operator

We begin with the case of a pseudo-scalar mediator denoted by P throughout this work. The general Lagrangian for a pseudo-scalar interaction is given as:

$$\mathcal{L}_P = \mathcal{L}_{SM} + \frac{1}{2}\Box P^2 - \frac{1}{2}M_P^2 P^2 + i\bar{\chi}\partial\!\!\!/_\mu \chi - m_\chi \bar{\chi}\chi - i g_{\chi P} P \bar{\chi}\gamma^5 \chi - \sum_q i g_{qP} \frac{y_q}{\sqrt{2}} P \bar{q}\gamma^5 q \quad (3.3)$$

Here, $\mathcal{L}_{SM}$ is the SM Lagrangian, $\Box$ is the d'Alembert operator ($= \partial^\mu \partial_\nu$), M_P is the mass of the mediator P, m_χ is the mass of χ, and $g_{\chi P}$ is the coupling of χ and P. g_{qP} is the constant describing the mass-dependent couplings of the mediator P with quarks (q) such that:

$$g_{qP} = g \frac{y_q}{\sqrt{2}} \quad (3.4)$$

where, y_q is the SM Yukawa coupling of the quarks such that $y_q/\sqrt{2} = m_q/v$. g is a real constant. The choice of the quark couplings proportional to their masses is to preserve chiral symmetry of the SM fermion masses [10, 13]. This definition of g_{qP} also comes in handy for coupling ratio-based analysis which we discuss in later chapters.

To derive the EFT operator we break down this Lagrangian. For a many body problem in quantum field theory, the S-matrix gives all the information of initial and final states in a process. This S-matrix forms the effective action when integrated over time. The effective action S, is given as:

$$S = \int d^n x \mathcal{L} \tag{3.5}$$

where, n is the number of space-time dimensions of the process and $\mathcal{L}$ is the Lagrangian describing all the interactions of ϕ. For the following derivation we use the basic axiom of four dimension, i.e. $n = 4$.

The correlational function of a particle 'ϕ', is then given by its path integral over the time limit from 0 to ∞ as:

$$e^{iS} = \int [d\phi_n]\, e^{iE(\phi_1\phi_2\ldots\phi_t)} \tag{3.6}$$

Here, ϕ_t describes the particle ϕ's states at different time intervals from 1 to t and E is its corresponding energy.

For a single field (ϕ) in the presence of an external source (J), the generating functional (Z) of the correlation function is given by [56]:

$$Z(J) = e^{-iE(J)} = \int \mathcal{D}\phi e^{\int d^4x(\mathcal{L}+J)} \tag{3.7}$$

Here, $\mathcal{D} = \prod_i d\phi_i$.

For an effective vertex with two incoming quarks, two outgoing WIMPs, and one pseudo-scalar mediator getting exchanged, we have in total five external sources. In our case, these are four fermionic fields (f) and one pseudo-scalar field (p). Thus, our generating functional of eq.(3.7) becomes:

$$Z(J) = Z(f_1, f_2, f_3, f_4, p) \tag{3.8}$$

$$= \int \mathcal{D}q\mathcal{D}\bar{q}\mathcal{D}\chi\mathcal{D}\bar{\chi}\mathcal{D}P \exp\left[\int d^4x \left(\mathcal{L} + f_1 q + f_2\bar{q} + f_3\chi + f_4\bar{\chi} + pP\right)\right] \tag{3.9}$$

Here, f_1, f_2, f_3, f_4 and p are the external source terms for the four fermions and one pseudo-scalar. This generating functional can now be used to calculate the path integrals.

Now, the general two-point correlation function for ϕ from state x to y is given as:

$$\langle\Omega|T\phi(x)\phi(y)|\Omega\rangle = \frac{Z[J]}{Z[0]} = \lim_{T\to\infty(1-i\epsilon)} \frac{\int \mathcal{D}\phi\phi(x)\phi(y)e^{i\int_{-T}^{T} d^4x\mathcal{L}}}{\int \mathcal{D}\phi e^{i\int_{-T}^{T} d^4x\mathcal{L}}} \tag{3.10}$$

where, $|\Omega\rangle$ denotes the ground state of the interaction, and T is time-ordering symbol. Also, $Z[J] = Z[0]$ when all the external fields are zero, i.e. $J = 0$.

Therefore,

$$\langle\Omega|T\phi(x)\phi(y)|\Omega\rangle = \frac{1}{Z_0}\left(-i\frac{\delta}{\delta J(x)}\left(-i\frac{\delta}{\delta J(y)}\right)Z[J]\right)\Big|_{J=0} \tag{3.11}$$

Here, the functional derivative is

$$\frac{\delta}{\delta J(x)}\int d^4yJ(y)\phi(y) = \phi(x) \tag{3.12}$$

Also,

$$\frac{\delta}{\delta J(x)}J(y) = \delta^4(x-y) \tag{3.13}$$

Thus, we have

$$\langle\Omega|T\phi(x)\phi(y)|\Omega\rangle = D_\phi(x-y) \tag{3.14}$$

Here, $D_\phi(x-y)$ is Green's function describing the propagator for a field from point x to y. For our pseudo-scalar mediator (P), the Green's function is denoted as $D_P(x-y)$.

We now discuss our calculations for pseudo-scalar and fermionic functional parts separately. Let us denote $\mathcal{D}q\mathcal{D}\bar{q}\mathcal{D}\chi\mathcal{D}\bar{\chi}$ together by $\mathcal{DF}$, and all the fermionic parts of the Lagrangian by F. Now, we first calculate the mediator dependent part of the Lagrangian. The integral for e^{iS} has a square term for the pseudo-scalar field P coming from the Lagrangian in eq.(3.3). We can generate this term by using following transformation as:

$$P(x) \to P(x) - i\int d^4yD_P(x-y)F(y) \tag{3.15}$$

Using this we can thus write

$$\begin{aligned}\mathcal{L}_{P+interaction} = -\frac{1}{2}\Big[P(x) - i\int d^4yF(y)D_P(y-x)\Big]\Big[\Box + {M_P}^2\Big] \\ \Big[P(x) - i\int d^4zF(z)D_P(z-x)\Big] - \frac{i}{2}\int d^4yF(x)D_P(x-y)F(y)\end{aligned} \tag{3.16}$$

Coming to the fermionic part of the functional, we use the following transformation:

$$F(x) \to F(x) + \int d^4yD_F(x-y)F(y) \tag{3.17}$$

Similarly, the fermionic part will be:

$$\begin{aligned}\mathcal{L}_F = \Big[F\bar{(}x) + \int d^4yF\bar{(}y)S_F(y-x)\Big]\Big[i\partial\!\!\!/ - m_F\Big] \\ \Big[F(x) + \int d^4zF(z)S_F(z-x)\Big] - \int d^4y\mathcal{F}(x)S_F(x-y)\mathcal{F}(y)\end{aligned} \tag{3.18}$$

The Green's function has the following properties for pseudo-scalar field:

$$(\Box + M_P^2)D_P(x-y) = -i\delta^4(x-y) \tag{3.19}$$

$$D_P(y-x)(\Box + M_P^2) = -i\delta^4(x-y) \tag{3.20}$$

and, for fermionic field:

$$(i\partial\!\!\!/ - m_F)S_F(x-y) = i\delta^4(x-y) \tag{3.21}$$

$$S_F(y-x)(i\partial\!\!\!/ - m_F) = i\delta^4(y-x) \tag{3.22}$$

Using the Gaussian path integral for the field independent terms of pseudo-scalar part, we get:

$$\int \mathcal{D}P \exp\Big(-\frac{1}{2}\int d^4x P(x)[\Box + M_P{}^2]P(x)\Big) = \det[\Box + M_P^2]^{-1/2} \tag{3.23}$$

Similarly for the fermionic part we get:

$$\int \mathcal{D}\mathcal{F}\mathcal{D}\bar{\mathcal{F}} \exp\Big(\int d^4x \bar{F}(x)[i\partial\!\!\!/ - m_F]F(x)\Big) = \det[i\partial\!\!\!/ - m_F] \tag{3.24}$$

The above constant mass terms and the interaction independent fermionic terms will cancel out when substituted in eq.(3.10). Thus, we can write our generating functional consisting of only the interaction part as:

$$Z[J] = Z[F,P] = e^{i\int d^4x\mathcal{L}} = \exp\int d^4x\Big[-\frac{i}{2}F(x)D_P(x-y)F(y)\Big] \tag{3.25}$$

In the above steps, we have been successfully able to extract our mediator out from the interaction. The action $e^{i\int d^4x\mathcal{L}}$ can also be defined in momentum space by using Fourier transformation. Using this in the above equation we get:

$$F(x) = \int \frac{d^4k}{(2\pi)^4}\tilde{F}(k)e^{-ikx} \tag{3.26}$$

Also, the Green's functional, in terms of the momentum exchanged between the particles (Q), then becomes:

$$D_P(x-y) = \int \frac{d^4Q}{(2\pi)^4}\frac{1}{Q^2 - M_P^2}e^{-iQx} \tag{3.27}$$

Integrating the exponential terms gives:

$$\int d^4x e^{ikx} = (2\pi)^4\delta^4(k) \tag{3.28}$$

Thus, substituting the above transformed terms into the integral of the generating functional, eq.(3.6), we get:

$$iS = \frac{i}{2}\int \frac{d^4Q}{(2\pi)^4}\tilde{F}(-Q)\frac{1}{Q^2 - M_P^2}\tilde{F}(Q) \tag{3.29}$$

Now, for the validity of our EFT implementation, and to ensure the production of the mediator as off-shell, we know that the minimal condition is

$$Q^2 - M_P^2 \approx -M_P^2 \tag{3.30}$$

On applying this condition and by using Taylor's expansion, we get:

$$\frac{1}{Q^2 - M_P^2} = -\frac{1}{-M_P^2} + \frac{Q^2}{M_P^4} + \textit{higher order terms} \approx \frac{1}{M_P^2} \tag{3.31}$$

Thus, on transforming back from the momentum space to real physical space we get:

$$iS = \frac{1}{2}\frac{1}{M_P^2}\int d^4x(F(x))^2 \tag{3.32}$$

With this, our effective Lagrangian for the four point interaction can be interpreted as:

$$\mathcal{L}_{eft} = \frac{1}{M_P^2}F(x)^2 \tag{3.33}$$

Now, from the initial Lagrangian, we know that F consists of WIMPs (χ) and quarks (q) in our EFT model. Thus, for the pseudo-scalar interaction, we can finally write our effective operator as:

$$\mathcal{O}_{PS} \equiv \frac{g_{\chi P}g_{qP}}{M_P^2}(\bar{\chi}\gamma_5\chi)(\bar{q}\gamma_5 q) \tag{3.34}$$

The cut–off scale, Λ_{PS}, which we consider equal for all quarks (with non–vanishing coupling to P), is now given by:

$$\Lambda_{PS}^3 = \frac{M_P^2 m_q}{g_{qP}g_{\chi P}} = \frac{vM_P^2}{gg_{\chi P}} \tag{3.35}$$

where, $v \simeq 246$ GeV is the vacuum expectation value of the Higgs field breaking the electroweak gauge symmetry. Note, that here we have assumed that the theory is weakly coupled, i.e. that the total decay width of the mediator, Γ_P, is significantly smaller than its mass, $\Gamma_P^2 \ll M_P^2$.

Thus, the dimension-6 effective operator for pseudo-scalar interaction is finally given as:

$$\mathcal{O}_{PS}^6 = \frac{m_q}{\Lambda_{PS}^3}\,(\bar{q}\gamma_5 q)\,(\bar{\chi}\gamma_5\chi) \tag{3.36}$$

3.2.2 Axial-vector operator

In this section, we derive the effective operator for the axial-vector mediator (A) with mass m_A. Again, our WIMPs (χ) are the Dirac fermions with mass m_χ, and the only SM fermions that the mediator will interact with are the quarks (q). The general Lagrangian in this case will be:

$$\mathcal{L}_A = \mathcal{L}_{SM} - \frac{1}{4}A^{\mu\nu}A_{\mu\nu} + \frac{1}{2}m_A^2 A^\mu A_\mu + i\bar{\chi}\gamma^\mu\partial_\mu\chi - m_\chi\bar{\chi}\chi + g_\chi A_\mu\bar{\chi}\gamma^\mu\gamma^5\chi + \sum_q g_q A_\mu \bar{q}\gamma^\mu\gamma^5 q \tag{3.37}$$

Here, $\mathcal{L}_{SM}$ stands for the SM Lagrangian. A is the axial-vector mediator with field strength tensor $A_{\mu\nu} = \partial_\mu A_\nu - \partial_\nu A_\mu$. g_{qA} and $g_{\chi A}$ are the couplings of the mediator to q and χ, respectively.

We follow the similar prescription for calculating the generating functional and the correlation functional as described in the previous section. Also, here the fermionic part of our functional is the same for χ is again a Dirac fermion.

The Green's functional for the axial-vector mediator is given as:

$$D_A{}^{\alpha\beta}(x-y)\Big[({M_A}^2 + \Box)g_{\beta\gamma} - \partial_\beta\partial_\gamma\Big] = i\delta^4(x-y)\delta^\gamma_\alpha \tag{3.38}$$

$$\Big[({M_A}^2 + \Box)g_{\alpha\beta} - \partial_\alpha\partial_\beta\Big]D_A{}^{\beta\gamma}(x-y) = i\delta^4(x-y)\delta^\alpha_\gamma \tag{3.39}$$

The above Green's functional in the momentum space looks like:

$$D_A{}^{\alpha\beta}(x-y) = \int \frac{d^4Q}{(2\pi)^4}\frac{-i}{Q^2 - M_A^2}\Big(\delta^{\alpha\beta} - \frac{Q^\alpha Q^\beta}{M_A^2}\Big)e^{iQ(x-y)} \tag{3.40}$$

The dummy indices cancel out after performing the complete Fourier analysis, and converting back to the real physical space. Thus, after implementing the limit on the momentum (eq.(3.30)), the final effective Lagrangian can be obtained as:

$$\mathcal{L}_{eft} = \frac{1}{M_A^2}F^\mu F_\mu \tag{3.41}$$

where, following from the previous section, F stands for the fermionic part of the generating functional. Thus, the effective operator for the axial-vector mediator is given by:

$$\mathcal{O}_{AV} \equiv \frac{g_\chi g_q}{M_P^2}(\bar{q}\gamma_\mu\gamma_5 q)(\bar{\chi}\gamma_\mu\gamma_5\chi) \tag{3.42}$$

Again, for a weakly coupled theory, the total decay width Γ_A of the mediator should be much smaller than its mass. The cut–off scale, Λ_{AV}, of the effective theory is then

$$\Lambda_{AV} = \frac{M_A}{\sqrt{g_{\chi A}g_{qA}}} \tag{3.43}$$

If Γ_A is not negligible, the numerator in eq.(3.43) is replaced by $[M_A^2\,(M_A^2 + \Gamma_A^2)]^{1/4}$. Later we will see that this can cause problems if M_A is significantly larger than Λ_{AV}.

Thus, the effective dimension–6 four-fermion operator corresponding to the Lagrangian (eq.(3.37)) is given as:

$$\mathcal{O}^6_{AV} = \frac{1}{\Lambda^2_{AV}}\,(\bar{q}\gamma_\mu\gamma_5 q)\,(\bar{\chi}\gamma^\mu\gamma_5\chi)\ . \tag{3.44}$$

CHAPTER 4

Methodology

In Large Hadron Collider (LHC) protons are accelerated to 99% speed of light. At these energies when the protons collide they break down into quarks, gluons and other fundamental particles. If WIMPs are also fundamental particles, there is a good probability for them to be created in such high-energy collisions. As WIMPs are significantly stable, they are always produced in pairs to avoid their immediate decay in the colliders. As WIMPs are sufficiently massive, one can detect a WIMP pair by observing a high-p_T object recoiling against it. As WIMPs are invisible to the detector material, this will create and imbalance in the total energy for an event. This transverse missing energy, E_T^{miss}, (or missing p_T), can then be manifested as the invisible WIMP pair. The high-p_T object could mainly be a photon, a boson (h, Z, W), or a gluon which further hadronizes into a high-energy jet [10, 11]. As the colliding beams in LHC are protons, the probability of WIMP production associated with a single high-energy jet (often called as a mono-jet) is higher compared to the other objects. Thus, for WIMPs at colliders the largest cross section and strongest bounds come from the mono-jet searches.

Thus, in order to detect the WIMP production in colliders, we look into the following process:

$$q + \bar{q} \rightarrow \chi + \bar{\chi} + g \tag{4.1}$$

Here, a quark pair ($q\bar{q}$) annihilates into a WIMP pair ($\chi\bar{\chi}$). A gluon (g) with high-p_T is required to be emitted as initial state radiation, thus producing a mono-jet like event. This 'hard' QCD jet gives a large amount of transverse momentum, hence approximately large E_T^{miss}. A Feynman diagram leading to this signature in the framework of the EFT is shown in Fig.(4.1). The cross-section (σ) for this process is given as:

$$\sigma \approx \frac{g^2_{q(P,A)} g^2_{\chi(P,A)}}{(M^2_{P,A} - Q^2)^2 + M^2_{P,A}\Gamma^2_{P,A}} \tag{4.2}$$

Here, the notations P, A correspond to the operators described in previous chapter, M is again the mass of the respective mediator, Q is the momentum exchanged in the process, and Γ is the width of the corresponding mediator.

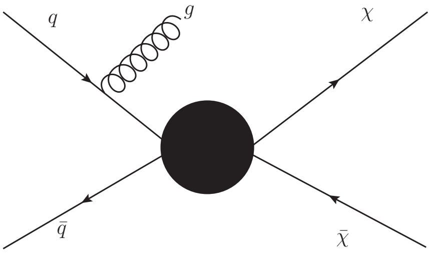

Figure 4.1: A Feynman diagram representation of a mono-jet event for the four–point EFT interaction vertex corresponding to eq.(4.1).

4.1 Analysis

In this section, we discuss in detail the mono-jet bounds at the LHC. We compare our results with both CMS (Compact Muon Solenoid) and ATLAS (A Toroidal LHC ApparatuS) detectors. Both the detectors use a right-handed coordinate system where the collision point at the center of the detector is the origin, the z-axis is along the beam pipe, the x-axis is from the interaction point towards the center of the LHC ring, and the y-axis points upwards from the ground. The azimuthal angle, ϕ, is always measured around the beam axis; the polar angle, θ, is measured with respect to the z-axis; and pseudorapidity is defined as $\eta = -ln[tan(\theta/2)]$. The transverse energy and momentum are defined as $E\ sin\theta$ and $p\ sin\theta$, respectively.

The CMS detector at LHC is a layered detector submerged in the high and localized constant magnetic field of a superconducting solenoid [57]. The detector has multiple layers; the first and innermost layer being the silicon pixel and strip tracker capable of reconstructing the path of most high-energy particles (e^-, μ, and hadrons) with a momentum resolution of 2% for $1 < p_T < 100\,\text{GeV}$. The tungsten electromagnetic calorimeter (ECAL), and the hadron calorimeter (HCAL) measure the energy of most of the particles within a pseudorapidity, $|\eta|= 5$. The muons are efficiently reconstructed with muon detection chambers, thus allowing a safe measure of their contribution to E_T^{miss}. The E_T^{miss} recorded by the experiments includes SM neutrinos, however, their count can accurately be measured by the information on all the other detectable particles and precise background estimation.

The largest detector at LHC is the ATLAS detector [58]. Similar to CMS, it has the innermost layer with silicon pixel detectors (PD), along with radiation trackers covering up a pseudorapidity range of $|\eta|< 2.5$. The calorimeter layer consisting of ECAL and HCAL together provide a coverage of $|\eta|< 4.9$. The muons are all reconstructed in the muon tracker which covers $|\eta|< 2.7$.

We use our EFT model with axial-vector and pseudo-scalar mediators to validate our analysis by comparing our bounds on the scale Λ_{AV} and Λ_{PS} with the bounds derived by both the ATLAS and CMS collaborations. Since we wish to reproduce the EFT limit, we keep our choice of the off-shell mediator mass of 10 TeV, and its width of 1 GeV, such that eq.(3.43) is still applicable. For our analysis, we vary the WIMP mass as, $m_\chi = 1$, 100, 200, 400, 700, 1000 GeV.

We begin with writing the model files in FeynRules-v2.0 [59]. All the necessary model details for the particles and their couplings, along with the complete Lagrangian, are given as an input to FeynRules-v2.0. As our model is based on EFT, the only required parameters are the WIMP mass (m_χ), the mediator mass ($M_{P,A}$) and general cut-off scale (Λ) which further determines the couplings. Based on our EFT model, we have considered that the mediator couples only to quarks and WIMPs equally for the axial-vector interaction. We define the Lagrangian as in eq.(3.37) and include the SM model available in FeynRules-v2.0. We introduce that the interaction between the q and χ is carried by the mediator A (or P) coming from 'New Physics' (NP). We use the acronym 'NP' in our model file to limit the interaction order of new physics to NP $= 1$, i.e., we allow at least one NP vertex or in other words, at least one mediator exchange in the interaction.

The output from FeynRules, describing all the possible interactions in the Universal FeynRules Output (UFO) format [60], is then used as an input to MadGraph5-aMC.at.NLO.v2.3.0 [61], a Monte-Carlo tool [62, 63] for matrix element calculations and event generation. The mono-jet signal requires the existence of at least one hard jet. We therefore allow events with at least one additional jet for increased efficiency. We use the MSTW2008LO set of parton densities [64] as implemented in the LHAPDF package [65]. Using MadGraph, we generate the following process with 1-2 partons in the final state as:

> generate p p > χ $\bar{\chi}$ j @1 NP=2 QCD=2 QED=0

> add process p p > χ $\bar{\chi}$ j j @2 NP=2 QCD=2 QED=0

where, j @1 limits the number of jets allowed. The conditions NP=2, QCD=2 and QED=0 limit the coupling orders of NP, QCD and QED, respectively. QED=0 allows us to neglect any electroweak jet contribution. For the generation of MadGraph events, we set number of NP vertices, $N_{NP} = 2$ (or NP=2 in the MadGraph notation) as this allows to limit only a single exchange of the mediator in the process. Note that increasing the number of jets affects the signal sensitivity, however, we limit the jet production to only two jets at the matrix element level in order to have an increased efficiency for the signal after the final cuts.

Similar to cross-sections of processes involving jets at hadron colliders, our cross-section will diverge as the p_T of the jets goes to zero. The experimental mono-jet searches use strong cuts on the E_T^{miss} and on the p_T of the hardest jet. Therefore, we apply parton-level cuts at MadGraph level of minimum $p_T = 200\,$GeV for the leading jet, and minimum $E_T^{miss} = 300\,$GeV. This choice also allows our events to completely satisfy the trigger level cuts in the experiments which are 105 GeV and 80 GeV for E_T^{miss} and leading jet p_T, respectively. The random seed number is kept the same for all the events which helps in minimizing any fluctuations in the final results occurring merely due to generator settings. To avoid any further stringent constraints at the parton level we keep all the other cuts equal as the defaults defined for the respective quantities in MadGraph. In MadGraph, the definition of E_T^{miss} only includes neutrinos. As in our study for mono-jets we require only the WIMPs to account for E_T^{miss}, we redefine E_T^{miss} in MadGraph by including χ and $\bar{\chi}$.

For parton showering, the generated events are passed to PYTHIAv6.4 [66], which is integrated with MadGraph5-aMC.at.NLO.v2.3.0. Hard parton showering off the $\chi\bar{\chi}$ plus one parton sample of MadGraph events, leads to the same final state as $\chi\bar{\chi}$ plus two parton MadGraph events with relatively soft showering. In order to remedy this double counting, we use the Michelangelo L. Mangano (MLM) matching prescription [67] for jets, also implemented in MadGraph5-aMC.at.NLO.v2.3.0. The MLM matching prescription allows to control the breakdown of matrix element for soft partons and showering for hard partons. To regulate the overlapping of soft partons coming from matrix element and the hard partons from showering, the MLM prescriptions introduces the parameter *xqcut*. *xqcut* separates the region of phase space to be populated by showering from that to be populated by the second hard parton, explicitly generated by MadGraph. We checked that varying the value of *xqcut* up to a factor of two has little impact, both at the parton-level cross-sections and also on the final cross section, after all the detector level cuts are applied. Hence, we use a value of 100 GeV for the *xqcut* variable. Since our generator-level cuts are quite strong, this choice of *xqcut* ensures that the efficiency for passing the final cuts is not very low. We found it sufficient to generate $50,000$ events per point of the parameter space.

In order to implement the final selection cuts for various mono-jet signal regions as well as a (simplified) simulation of detector effects we use CheckMATE-v2.0 [68, 69], based on Delphes-v3.0.10 [70] with modified detector cards, as well as Fastjet-v3.0.6 [71] for the jet reconstruction. We implemented CMS [12] and ATLAS [13] mono-jet analysis for $\sqrt{s} = 8\,\text{TeV}$ in CheckMATE-v2.0, following the prescription of [72].

4.1.1 Implementation of CMS 8 TeV analysis

The CMS 8 TeV mono-jet analysis has a luminosity of 19.6 fb^{-1} [12]. The reconstruction of all the particles produced in an event and background estimation have been described in detail by the experiments. The experimental analysis divides the signal regions into seven parts with the lower bound on the E_T^{miss}, such that $E_T^{miss} >$ 250, 300, 350, 400, 450, 500 and 550 GeV. We stick to this distribution for consistency. To include all the systematic and statistical uncertainties for precise final results, CheckMATE allows the statistical evaluation using the CL prescription [73]. For this we give the input data on the statistical and systematic uncertainties in the CheckMATE analysis manager. As CMS provides the data at 90% C.L., we derive these limits from the full CLs limits (95% C.L.) obtained using CheckMATE. The selection criteria implemented in CheckMATE using *AnalysisManager* are given below:

1. All jets are required to have a minimum $p_T > 20\,\text{GeV}$. As required by FastJet anti-*kt* algorithm [74], all jets are constructed within a cone radius, $R = 0.5$.

2. To guarantee a mono-jet like event, atleast one single jet with high p_T is required to accommodate for the E_T^{miss}. Thus, leading jet with highest p_T is required to have $p_T > 110\,\text{GeV}$ and $|\eta| < 2.4$.

3. A second jet is accepted only if it has $p_T > 30$ GeV and $|\eta| < 4.5$. Also, it should have a clear azimuthal separation from the leading jet, i.e. $\Delta\phi(j_1 j_2) < 2.5$ radians (or 143 degrees). This makes sure that the mono-jet event is not mistaken for a di–jet event.

4. To ensure that leading jet qualifying as mono-jet has pure BSM origin, any hard jet coming from QCD-like event is vetoed. For this, events with more than two jets are discarded when their $p_T > 30\,\text{GeV}$ and $|\eta| < 4.5$.

5. Lepton isolation criteria discards any lepton which does not contribute to jet composition. The cone radius along the direction of the lepton is defined as $\sqrt{\Delta\eta^2 + \Delta\phi^2} = 0.4$. A lepton is considered isolated if within this defined cone,

$$\frac{\sum p_{T\,\text{hadrons+photons}}}{p_{T\,\mu,e^-}} < 0.2 \tag{4.3}$$

   - Any electron or muon with $p_T > 10\,\text{GeV}$ and $|\eta| < 2.4$ is considered isolated and is discarded. In CheckMATE, $|\eta|$ can be implemented using the *FilterPhaseSpace* function. Also, CheckMATE predefines electrons as loose, medium and tight, similar to ATLAS' analyses. Here we apply the $|\eta|$ condition to *electronsMedium* as they fit better into the CMS isolation criteria which otherwise, does not distinguishes between the electrons. For muons, we use the *muonsCombined* function.
   - Other leptonic contributions to jets are vetoed by excluding events with tau leptons having $p_T > 20\,\text{GeV}$ and $|\eta| < 2.3$.

4.1.2 Implementation of ATLAS 8 TeV analysis

The ATLAS 8 TeV mono-jet analysis [13] with luminosity of 20.3 fb^{-1}, is very similar to the CMS in the approach, although it has few definitions and signal choices different than CMS. Again, for consistency of our results, we consider the similar signal regions as defined by ATLAS. ATLAS divides the signal regions (SRs) into nine regions, SR1 to SR9, such that they have minimum E_T^{miss} of 150, 200, 250, 300, 350, 400, 500, 600 and 700 GeV. Again, all the systematic and statistical uncertainties are calculated by CheckMATE using the data provided by the experiment. As CheckMATE calculates the theoretical limits at 95% C.L. we can directly compare them with the ATLAS' limits at 95% C.L. The major signal selection cuts implemented are given below:

1. All jets are required to have a minimum $p_T > 30\,\text{GeV}$ and should be within $|\eta| < 4.5$. Also, based on FastJet anti-kt algorithm, all defined jets have a cone radius of $R = 0.4$.

2. The leading jet with highest p_T must have a $p_T > 120\,\text{GeV}$ and $|\eta| < 2.0$.

3. Mono-jet event is ensured with the condition that the p_T of the hardest jet is at least 50% of the total E_T^{miss}, i.e.,

$$\frac{p_{T\text{leading jet}}}{E_T^{miss}} > 0.5. \tag{4.4}$$

4. ATLAS does not apply a limit on number of jets in an event but ensures an azimuthal separation between all the jets and their E_T^{miss} (or missing transverse momentum, p_T^{miss}), i.e., $\Delta\phi$ (jet, p_T^{miss}) > 1 radian (57 degrees).
5. The E_T^{miss} is also required to be evaluated within a $|\eta|< 4.9$.
6. Lepton isolation criteria:
    - Muons with $p_T > 7\,\text{GeV}$ and $|\eta|< 2.5$ are isolated if the transverse momenta of non-muon tracks, confined in a cone of radius $\Delta R = 0.2$ around the muon, is less than 1.8 GeV.
    - Any electron with $p_T > 7\,\text{GeV}$ and $|\eta|< 2.47$ is considered isolated and is discarded.
    - A track is isolated if within $\delta R = 0.4$ there is no additional track with atleast a $p_T > 3\,\text{GeV}$. Any isolated tracks with $p_T > 10\,\text{GeV}$ and $|\eta|< 2.5$ is discarded in order to remove any unidentified lepton.

The signal efficiency is heavily dependent on the accurate estimation of all the background contributions. The backgrounds for both the experiments are very similar. For mono-jet signals, the backgrounds majorly come from electroweak processes, like $Z(\nu\nu)+$ jets and $W(l\nu)+$ jets, along with $Z(ll)+$ jets, QCD multi-jets and di-boson events. Precise estimation of neutrinos contributing to the missing energy is done by measuring neutrino background using $Z(\nu\nu)/W(l\nu)+$ jets control samples. For all the contributions Monte-Carlo simulations are performed with relatively relaxed selection cuts compared to the cuts on the signal event. This data forms the 'control regions', which are further used to normalize the actual data and uncertainties. CheckMATE offers to evaluate the background contributions by offering the implementation for these control regions provided by the experiments. However, we do not require any control regions or background simulations for our analysis since we focus only on the implementation of the signals.

4.1.3 Implementation of ATLAS 13 TeV analysis

For the early (2015) $\sqrt{s} = 13\,\text{TeV}$ data, CMS does not provide any analysis for mono-jet bounds. Also, ATLAS does not use the EFT interpretation of their mono-jet bounds. Hence, we instead consider the simplified model analysis of ATLAS [75]. We implement their signal regions into CheckMATE-v2.0 and test our effective model against this search. ATLAS achieved a luminosity of 3.2 fb^{-1} for $\sqrt{s} = 13\,\text{TeV}$. For 13 TeV search, ATLAS describes the signal regions as exclusive and inclusive. For our work, we explore the inclusive signal regions as they are in order with the 8 TeV analysis and appropriate for being translated into model-independent upper limits on the cross-section. These inclusive signal regions are divided into seven parts, such that their $E_T^{miss} > 250, 300, 350, 400, 500, 600, 700\,\mathrm{GeV}$.

As the trigger for E_T^{miss} at this increased center of mass energy at ATLAS is 250 GeV, we keep our parton level cuts at the MadGraph level same as before, as the final signal events with the at least one jet of $p_T > 200\,\mathrm{GeV}$ and $E_T^{miss} > 300\,\mathrm{GeV}$ satisfy the above trigger. The signal selection criteria are given below:

1. All jets are required to have a minimum $p_T > 20\,\mathrm{GeV}$, should be within $|\eta| < 2.8$ and are constructed within a cone of radius, $R = 0.4$.
2. The leading jet with highest p_T must have a $p_T > 250\,\mathrm{GeV}$ and $|\eta| < 2.4$.
3. Like ATLAS, we allow maximum four jets only if they have a $p_T > 30\,\mathrm{GeV}$ and $|\eta| < 2.8$. They are required to have clear azimuthal separation such that $\Delta\phi(jet, p_T^{miss}) < 0.4$.
4. Any electron with $p_T > 20\,\mathrm{GeV}$ and $|\eta| < 2.47$, and a muon with $p_T > 10\,\mathrm{GeV}$ and $|\eta| < 2.5$, are considered isolated and are discarded.

The most sensitive signal regions used to set the final cuts, typically have $E_T^{miss} > 400$ or 500 GeV. It is important to note that neither ATLAS nor CMS strictly speak of pure mono-jet events. Vetoing events with a second reconstructed jet would reduce the signal considerably, since many events with $E_T^{miss} \sim 500$ GeV produce at least one additional jet from showering.

Results for the 8 TeV analyses are depicted in Fig.(4.2). We successfully reproduce the experimental lower bound on the cut-off scale (Λ_{AV}) to better than 10%. From this figure, the CMS limit looks more stringent than that of ATLAS. Note, however, that ATLAS quotes a lower bound at 95% C.L., whereas CMS only requires 90% C.L..

At the increased center of mass energy, $\sqrt{s} = 13\,\mathrm{TeV}$, the on-shell production of the mediator is in principle possible. However, from our results, we found that this contribution is negligible because of the very small parton densities at the required large parton energies. The resulting bound is shown in Fig.(4.4). We see that the lower bound on the cut-off scale strengthens by approximately 100 TeV for $\sqrt{s} = 13\,\mathrm{TeV}$ than those for $\sqrt{s} = 8\,\mathrm{TeV}$.

Formally, our set-up can also treat the pseudo-scalar case, by simultaneously choosing a large mediator mass, a small mediator width, and very large values for the coefficient g defined in eq.(3.4). We compare our bounds on the pseudo-scalar mediator to the ATLAS' scalar mediator bounds at $\sqrt{s} = 8\,\mathrm{TeV}$, Fig.(4.3). As the bounds for pseudo-scalar and scalar mediator are same at the high energy colliders at least for the low WIMP masses, are bounds are well within the 2-σ error for the low m_χ.

Owing to the factor of m_q in the coefficient of the pseudo-scalar four-fermion operator (eq.(3.36)), the resulting bound on Λ_{PS} is much weaker than in the axial-vector case. For example, even for light WIMPs, ATLAS quotes a lower bound on Λ_{PS} of $\sim 40\,\mathrm{GeV}$.

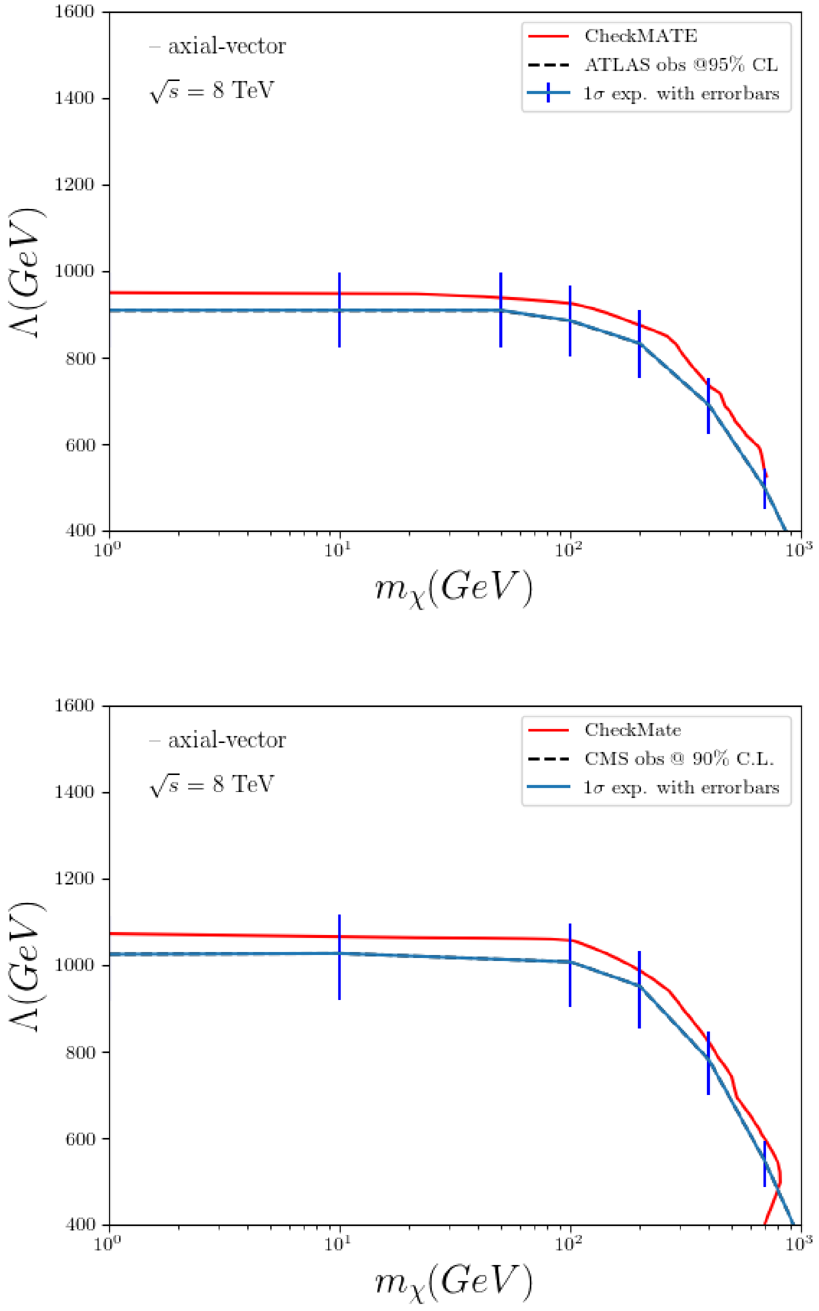

Figure 4.2: Our limits on the strength of the axial-vector interaction derived using CheckMATE, compared to the ATLAS limits on Λ_{AV} at 95% C.L. and CMS limits on Λ_{AV} at 90% C.L. for $\sqrt{s} = 8\,\text{TeV}$.

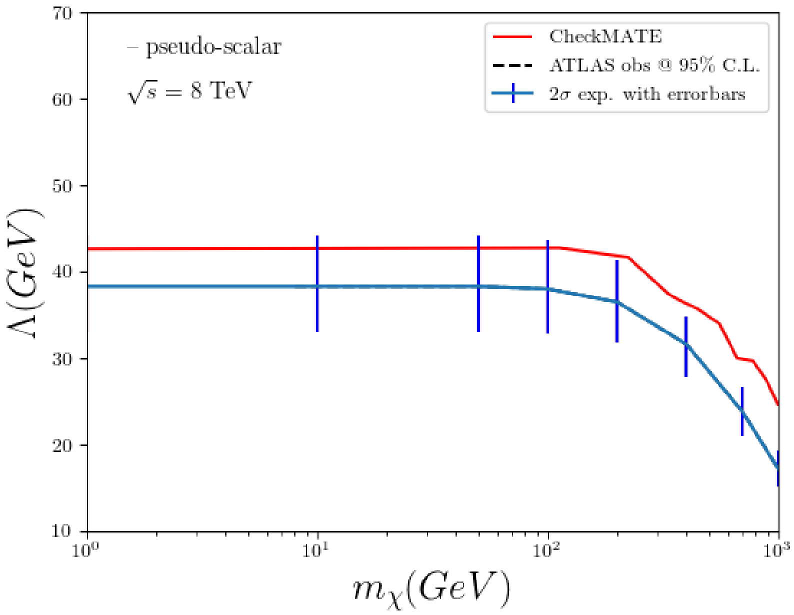

Figure 4.3: Our limits on Λ_{PS} derived using CheckMATE, compared to the ATLAS limits on scalar interaction at 95% C.L. for $\sqrt{s} = 8\,\text{TeV}$.

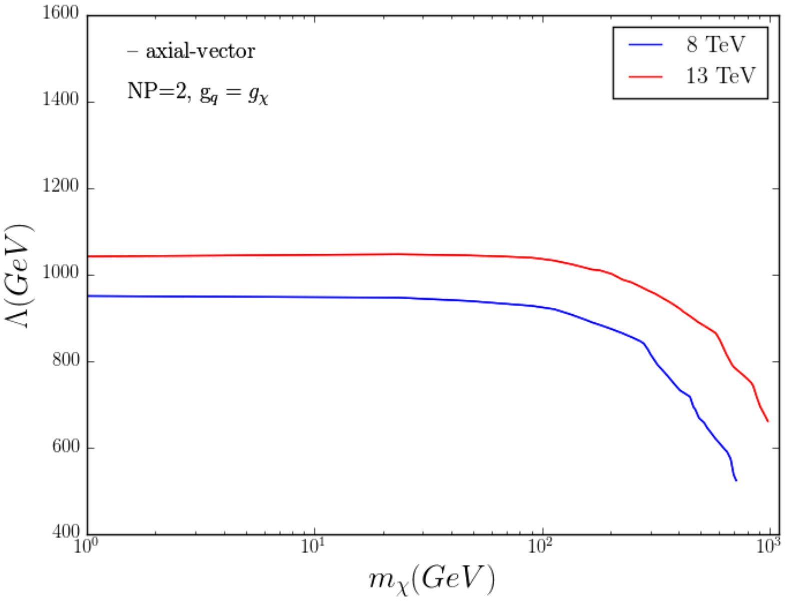

Figure 4.4: Bounds on Λ_{AV} for axial-vector interaction at 95% C.L. compared to the ATLAS data taken in 2015 at $\sqrt{s} = 13\,\text{TeV}$.

This is well below the values of even the basic acceptance cuts defining mono-jet events, making the usefulness of an EFT description, in this case, a priori unlikely.

4.2 A Combined Analysis

In order to obtain stronger limits, we combine the data from both ATLAS and CMS since they give comparable bounds on Λ_{AV}. Both ATLAS and CMS use 'confidence level' method to set the limits [73, 76]. If the errors on the background of the two experiments are totally correlated, i.e., if both the errors are only due to the luminosity error, then the total error should be a fixed percentage of the total background. In this case, the relative error will not change when combining the results from the two experiments. The total errors, however, in both the experiments, also come from their systematic and statistical uncertainties which are calculated independently and are experiment specific. Hence, as the errors in the background estimate are not correlated between the experiments it is straightforward to combine the results.

To explain how we estimate the combined limits we briefly describe an example of combining ATLAS SR7 ($E_T^{miss} > 500\,\text{GeV}$) [13] with CMS SR7 ($E_T^{miss} > 550\,\text{GeV}$) [12]. ATLAS quotes an expected background of $1,030 \pm 60$ events in this signal region, and finds $1,028$ events. From this we compute an upper bound on the number of signal events at 95% CL, $N_{95,\text{ATLAS}} = 134$, to be compared with an upper bound of 146 events quoted by ATLAS. CMS expects 509 ± 66 events in their SR7, and observes 519 events. Our computed $N_{95,\text{CMS}} = 145$, whereas CMS cites a value of 142. Combining these SRs we have a total expected background of $1,539 \pm 89$ events, whereas the actual number of observed events is $1,547$. From this we compute a combined 95% CL upper bound on the number of signal events $N_{95,\text{combined}} = 198$, to be compared with the sum of the individual N_{95} values of 279 events. The proper statistical combination thus reduces the upper bound on the total number of signal events by about 30%.

In practice, we let CheckMATE select the two signal regions which are expected to have the best sensitivity, based on the expected number of background events. We combine only these two statistically independent SRs as they refer to different experiments. In this way, we avoid 'look elsewhere' problems that could arise if we combined all nine ATLAS signal regions with all seven CMS signal regions. The most sensitive signal region depends on the value of m_χ, which (for large mediator mass) basically fixes the kinematics of the process.

We find that the combination strengthens the bound on Λ_{AV} in the model with axial-vector mediator only very slightly. For example, for light WIMPs, $m_\chi = 1\,\text{GeV}$, and again only including contributions with $N_{NP} = 2$, we have a combined 95% C.L. lower bound of $\Lambda_{AV} > 970\,\text{GeV}$, compared to individual 95% CL lower bounds of 950 GeV for ATLAS and 900 GeV for CMS.

CHAPTER 5

Inconsistency of EFT Description

In this chapter, we discuss the interpretation of the mono-jet limits derived using EFT description in Chapter 4. We find that the results are internally inconsistent and discuss this in detail.

Recall the process generation in MadGraph for our analysis, eq.(4.1). Here we artificially restricted ourselves to only include the processes where a single mediator is exchanged by using $N_{NP} = 2$, in the language of MadGraph. For the description of such processes in EFT, the mediator masses are required to be very large and should also have very large couplings. These requirements might infer that the processes where two mediators are exchanged, i.e., $N_{NP} = 4$, might not be relevant enough to affect the results. We show, however, that these physically probable process with two mediators getting exchanged can considerably affect the current mono-jet bounds on WIMPs at the colliders.

For WIMPs in the final state, the second mediator can again couple to $\bar{\chi}\chi$ current. For a mono-jet like event, we will still require (at least) one hard parton from QCD interactions. A minimal example of $N_{NP} = 4$ interaction can be visualized in Fig.(5.1). Now, when the second mediator couples to a quark current, no QCD vertex is mandatory to produce a mono-jet signal. This is because the quarks are radiated off the first mediator which then goes to the second mediator, further decaying into a WIMP pair. These contributions will always have two partons (quarks or anti-quarks) in the final state. This is still consistent with our previous analyses, as we have seen that both ATLAS and CMS searches tolerate the existence of a second jet in their 'mono-jet' searches within certain limits.

For axial-vector case, this $N_{NP} = 4$ interaction will have a matrix element of order:

$$g_{\chi A} g_{qA}^3 \tag{5.1}$$

In case the mediator is emitted off the WIMP line, the matrix element will be of order:

$$g_{\chi A}^2 g_{qA}^2 \tag{5.2}$$

Thus, in general, the contribution of the second mediator exchange ($N_{NP} = 4$) in the

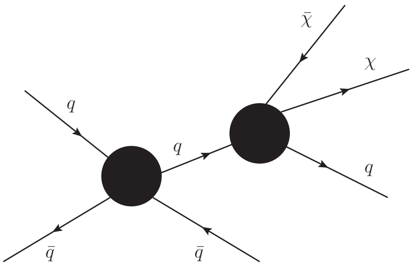

Figure 5.1: EFT interaction with $N_{NP} = 4$ having a double mediator exchange

total matrix element will look like

$$\mathcal{O} \approx (\Lambda^{-4}) \tag{5.3}$$

5.1 Axial-vector case

For axial-vector mediator, the product of the couplings in eq.(5.2) is fixed for all the processes once we fix $g_{\chi A}$ and g_{qA}, because we consider the couplings of A degenerate over the quark family in our EFT description. All $N_{NP} = 4$ contributions involve the propagator of light fermion (q or χ), in addition to the two mediator propagators. These contributions can therefore not be expressed as a single higher-dimensional operator. In some of these contributions, the momentum flowing through both of the boson propagators is space-like, in a sense that these are double $t-$channel mediators, rather than $s-$channel mediators. However, there are also several classes of contributions where the momentum flowing through both the mediator lines are time-like.

Using the techniques described in previous chapter, we generate the processes with second mediator exchange as:

> generate p p > χ $\bar{\chi}$ j @1 NP=4 QCD=2 QED=0

> add process p p > χ $\bar{\chi}$ j j @2 NP=4 QCD=2 QED=0

Keeping the basic assumptions of our EFT same as described in Chapter 3, we now compare the bounds on Λ_{AV}, from $N_{NP} = 4$ interactions with that of $N_{NP} = 2$, Figs.(5.2). For $N_{NP} = 4$ contributions, we see that the upper bound on Λ_{AV} increases by at least 40 GeV for the $\sqrt{s} = 8(13)$ TeV data, and 150 GeV for the $\sqrt{s} = 13$ TeV data. Now this increase of 40 GeV (about $\sim 5\%$) might not look very impressive. However, remember that the leading contribution to the signal cross-section scales like Λ_{AV}^{-4}. A 5% increase of the bound on Λ_{AV}, therefore, corresponds to a 20% increase of the total signal cross-section. This further implies that at $\sqrt{s} = 13$ TeV, the total cross-section increases by about 60%, Fig.(5.2).

The effect of the $N_{NP} = 4$ contributions becomes even more pronounced when we look at specific initial and final states. From the above discussion, it is clear that diagrams with double mediator exchange always have at least two partons in the final state. These diagrams will only contribute to the di-jet part of the signal cross-section,

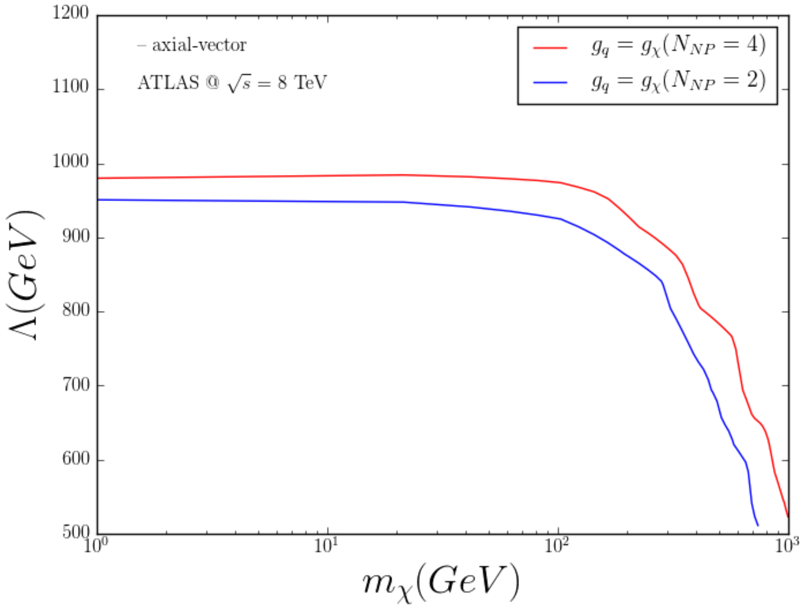

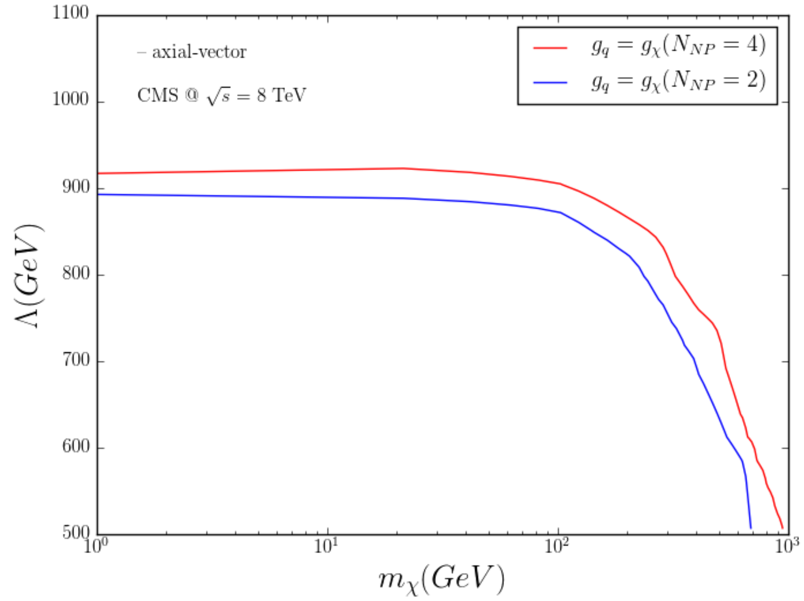

Figure 5.2: Comparison of bounds on Λ at 95% C.L. derived from ATLAS (up), and at 90% C.L. derived from CMS data (bottom), at $\sqrt{s} = 8\,\text{TeV}$. The blue curves are for $N_{NP} = 2$, i.e. only diagrams where a single mediator is exchanged are included, while the red curves for $N_{NP} = 4$ also include diagrams where two mediators are exchanged. Also, we have set $g_{\chi A} = g_{qA}$.

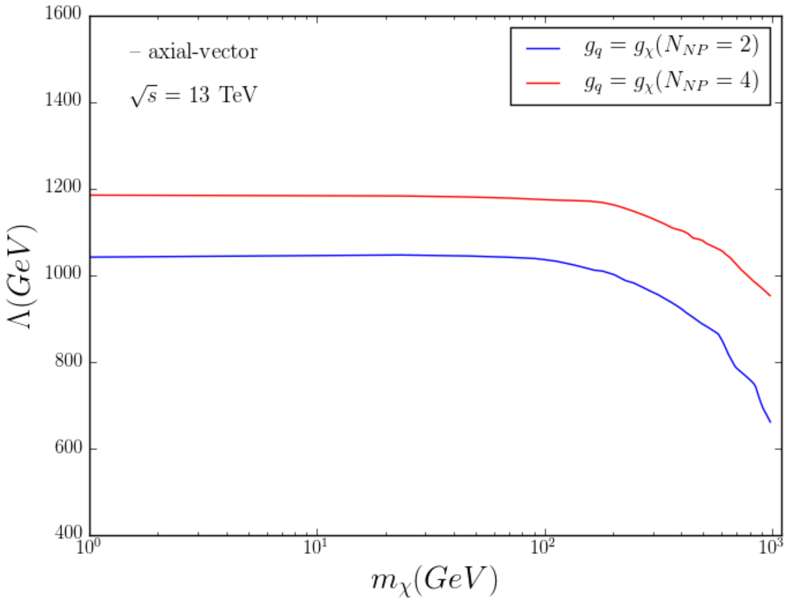

Figure 5.3: Comparison of bounds on Λ at 95% C.L. derived from ATLAS at 13 TeV. Again, here the blue curves are for $N_{NP} = 2$, i.e. only diagrams where a single mediator is exchanged are included, while the red curves also include diagrams where two mediators are exchanged ($N_{NP} = 4$). We have set $g_{\chi A} = g_{qA}$.

which contributes to about 25% of the total cross-section after matching, if only the generator-level cuts are applied. Moreover, $N_{NP} = 4$ contributions only exist if all external partons are (anti)quarks, rather than gluons, as restricted by our choice of the interactions. Thus, after the generator-level cuts, for $N_{NP} = 2$, all quark processes contribute about 15% to the total 'di-jet' cross-section, which is about 4% of the total signal cross-section.

The much stronger final ATLAS cuts enhance the importance of some of these contributions. In particular, contributions of the kind $qq \to \bar{\chi}\chi qq$ are the only ones with two valence quarks in the initial state. These contributions suffer the smallest reduction of the parton densities when the energy scale of the process is increased by increasing the E_T^{miss} cut. For this particular class of initial and final states, the effect of the $N_{NP} = 4$ contributions is very dramatic. For example, for $\Lambda_{AV} = 900\,\text{GeV}$ and $m_\chi = 1\,\text{GeV}$, the $N_{NP} = 4$ terms increase the cross-section for $uu \to uu\bar{\chi}\chi$ (where u stands for a u quark or anti-quark) by a factor of 2.7 even if only the generator–level cuts are applied. The impact of the $N_{NP} = 4$ contributions is even larger after the final cuts since the Λ_{AV}^{-4} suppression of these matrix elements implies that they become relatively more important when the energy scale of the process is increased. The relative importance of the $N_{NP} = 4$ contributions obviously increases with decreasing Λ_{AV}. Since the bound on Λ decreases with increasing WIMP mass, the impact of the $N_{NP} = 4$ contribution on the final bound is, therefore, even stronger for heavier WIMPs.

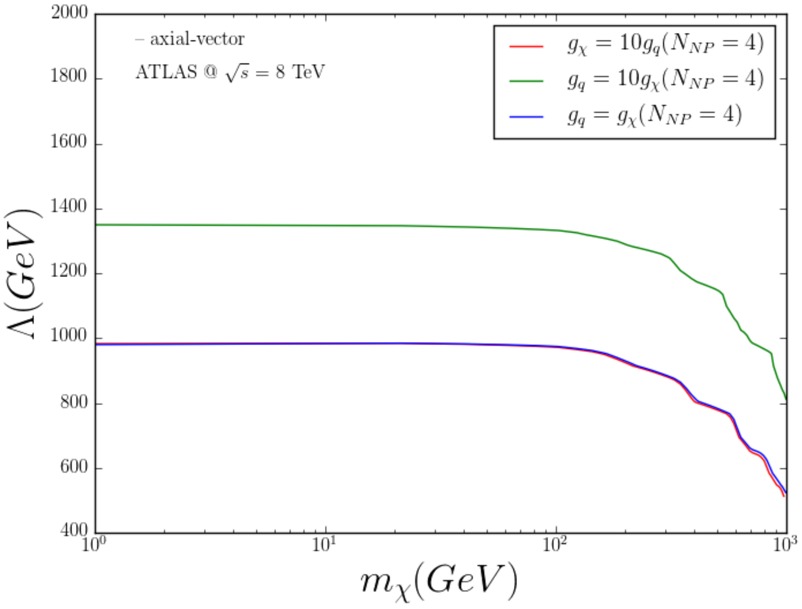

Figure 5.4: Comparison of ATLAS' bounds on Λ_{AV} at 95% C.L. for $N_{NP} = 4$ for different coupling ratios.

Table 5.1: Our ATLAS' and CMS' limits on Λ_{AV} for different coupling ratios at $\sqrt{s} = 8\,\text{TeV}$ based on $N_{NP} = 4$ processes.

Coupling ratios	$\Lambda_{AV,\text{ATLAS}}$ (GeV)	$\Lambda_{AV,\text{CMS}}$ (GeV)
$g_{\chi A} = g_{qA}, N_{NP} = 2$	950	900
$g_{\chi A} = g_{qA}, N_{NP} = 4$	980	950
$g_{\chi A} = 10 g_{qA}, N_{NP} = 4$	980	950
$g_{\chi A} = 0.1 g_{qA}, N_{NP} = 4$	1350	1250

The $N_{NP} = 4$ contributions depend on the coupling ratios of the mediator to q and χ. To demonstrate this, we consider different coupling ratios, i.e. $g_{\chi A} = g_{qA}$, $g_{\chi A} = 10 g_{qA}$ and $g_{\chi A} = 0.1 g_{qA}$ and derive our limits by keeping the remaining parameters same as used for our axial-vector EFT analysis at 8 TeV. The results are depicted in Fig.(5.4). We see that $g_{qA} > g_{\chi A}$ receives to quite a large contributions from $N_{NP} = 4$ processes. For $g_{qA} < g_{\chi A}$ these contributions are essentially negligible as there is a large suppression on the mediator-quark couplings. Thus, the $N_{NP} = 4$ limits in this case are roughly same as that for $g_{qA} = g_{\chi A}$. Our strongest limits coming from $g_{qA} = 10 g_{\chi A}$ for $N_{NP} = 4$ are below 2 TeV, hence, our results are always within the limits on four-quark interactions coming from QCD. Thus, for an $s-$channel mediator the 'mono-jet' limit is relevant only if $g_{\chi A}$ is significantly larger than g_{qA}. Table(5.1) summarizes the limits on Λ_{AV} based on $N_{NP} = 4$, and compares them with the standard limits coming from $N_{NP} = 2$.

The importance of these $\mathcal{O}(\Lambda^{-4})$ contributions to the matrix element of the signal basically dooms the EFT description. However, in the spirit of an EFT, for consistency one would have to add all contributions of order Λ^{-4}. This includes, in particular, contributions from operators of mass dimension up to 8 in the effective Lagrangian, of which there are a great many. The usual treatment of ignoring all $N_{NP} = 4$ contributions amounts to the assumption that the coefficients of all of these dimension-8 terms are negligible, which cannot be justified from the point of view of the EFT alone. Note that this is true already for the $\sqrt{s} = 8\,\text{TeV}$ data. We saw above that, not surprisingly, the effect of the $N_{NP} = 4$ terms is even larger for the 13 TeV data. Thus, with some important sub-processes contributing to the 'mono-jet' signal, including only the $\mathcal{O}(\Lambda^{-2})$ contributions to the matrix elements underestimates the current EFT bounds, where on-shell production of the mediator is negligible for the considered energies.

5.2 Pseudo-scalar case

The pseudo-scalar case is quite different from the axial-vector one. For example, since the bounds in the usual treatment are much weaker one would expect much bigger effects from using the NP vertex twice as the couplings are directly proportional to the quark masses. However, even treating this vertex once is non-trivial if we include loop induced processes, as one should if the ansatz for the couplings of the mediator to quarks also applies to the top quark. Also, inserting this kind of loop interaction twice is far more complicated.

It is easy to see that it does not make much sense to extend this model to the top sector, at least not in regions of parameter space anywhere near the current ATLAS and CMS mono-jet bounds. For example, ATLAS finds a lower bound on their scale Λ of about 40 GeV for light χ for the scalar case (scalar and pseudo-scalar are basically the same for small m_χ). Using the coupling of the mediator to quarks as in eq.(3.4), and Λ_{PS} in eq.(3.35), we can have,

$$g_{\chi P} g = v \frac{{M_P}^2}{\Lambda_{PS}^3} \tag{5.4}$$

As the couplings (and their products) are mass dependent, the $N_{NP} = 4$ contributions to the total matrix element for the signal will heavily depend on the coupling ratios of the mediator to quarks and WIMPs. The ATLAS' bound in this channel requires $E_T^{miss} > 500\,\text{GeV}$. Hence, the EFT approach will only make sense if, very conservatively, the pseudo-scalar mass is above 500 GeV. On the other hand, for $M_P > 500\,\text{GeV}$ and $\Lambda_{PS} = 40\,\text{GeV}$, we get $g_{\chi P} g > 680$. Recalling that $v \simeq m_t$, this implies that for our model to saturate the ATLAS bound for a mediator mass, where the EFT might not be completely off, requires the product of the couplings of the mediator to the χ and top quark to exceed 500. Hence, it will not be possible to build a perturbative theory in this case.

In order for the cross-section not to be dominated by the on-shell production of the mediator, one indeed needs mediator mass to be a few TeV. Recall that for fixed Λ the pseudo-scalar coupling scales like M_P^2, even if the couplings of the mediator and quarks will have to be non-perturbative near the present experimental bound. In order to make this last point a little bit more quantitative, we further consider a variant of the model in next chapter for different mediator widths and determine the conditions for which a simplified theory may be derived from our effective theory.

CHAPTER 6

A Simplified Model from EFT

We now compare our EFT results with a more realistic situation - a real ‘simplified model’ where the decay width of the mediator can be derived and calculated precisely [27, 77, 78]. We derive our simplified model from the parameters based on our EFT description. We discuss our model separately for the axial-vector and pseudo-scalar interactions separately. We first discuss the extent to which our simplified models can be accurately described by an EFT as far as mono-jet production is concerned, taking the finite width of the mediator into account. We further discuss other limits on the models, independent of the mono-jet interpretations.

6.1 Model descriptions

Our simplified models consist of SM quarks(q), and the WIMP sector which has an axial-vector mediator (A) of mass (M_A) = 10 TeV and spin 1, and a pair of WIMPs (χ) which are Dirac fermions and have a mass (m_χ) of 1 GeV. The off-shell mediator connects the SM quarks to the WIMPs by $s-$channel exchange. Similar to our EFT consideration we take the couplings of the mediator degenerate to all quarks g_{qA} and WIMPs $g_{\chi A}$. These couplings can be determined by fixing the energy scale of the theory (eq.(3.43)). Based on the current verified bounds on the cut-off scale, we have $\Lambda_{AV} = 900\,\text{GeV}$.

For our model with a pseudo-scalar mediator (P), we again take a mass (M_P) of 10 TeV and spin 1. WIMPs, again, are Dirac fermions of mass (m_χ) of 1 GeV. We again consider only the $s-$channel exchange. The couplings of the mediator to quarks are g_{qP} and $g_{\chi P}$, given by eq.(3.4), and can also be determined by eq.(3.35) after fixing $\Lambda_{AV} = 40\,\text{GeV}$.

In a simplified model, the width of the mediator (Γ) is finite and can be given as[1]:

$$\Gamma_A = \frac{M_A}{12\pi}\Big[g_{\chi A}^2\Big(1-\frac{4m_\chi^2}{M_A^2}\Big)^{3/2} + N_c g_{qA}^2 \sum_q \Big(1-\frac{4m_q^2}{M_A^2}\Big)^{3/2}\Big] \tag{6.1}$$

---

[1] see Appendix for details

$$\Gamma_P = \frac{M_P}{8\pi}\Big[g_{\chi P}^2\Big(1-\frac{4m_\chi^2}{M_P^2}\Big)^{1/2} + N_c g^2 \sum_q \frac{m_q^2}{v^2}\Big(1-\frac{4m_q^2}{M_P^2}\Big)^{1/2}\Big] \tag{6.2}$$

Here, the subscripts denote the corresponding particles in the respective models described above. Also, $v = 246\,\mathrm{GeV}$, m_q denotes the respective quark mass, $N_c = 3$ for colored quarks, and 1 for WIMPs.

6.2 Finite Width Effects and Applicability of the EFT

So far we have simultaneously chosen large masses (10 TeV) and small widths (1 GeV) for our $s-$channel mediators. This allows to reproduce the EFT limit in our formalism; note that FeynRules does not allow to directly input four–fermion operators into the Lagrangian. We also show that the current LHC bound on the scale Λ is about a TeV for the axial-vector mediator, and only about 40 GeV for the pseudo-scalar mediator, even for light WIMPs; for heavier WIMPs the bounds become even weaker. However, requiring the mediator mass to be significantly larger than Λ also requires couplings which are larger than 1. This, in turn, leads to large widths of the mediator. In other words, the combination of a large mediator mass $M^2 \gg \Lambda^2$ with a small mediator width $\Gamma^2 \ll M^2$ cannot be realized in a physical model.

For this discussion, our χ has mass 1 GeV. As noted in previous chapters, for heavier χ the bound on Λ is weaker which makes the problem even more severe. This means that the mediator can always decay into WIMPs as well as into quarks. If the decay into WIMPs was not possible, one could have generated a small width of the mediator by choosing its coupling to quarks to be very small. In order to keep Λ fixed, the coupling strength to WIMPs would then have to be increased such that the product of the couplings is constant. This quickly would require couplings to the WIMP exceeding $\sqrt{4\pi}$, again indicating that at least one sector of the model is not perturbative.

Evidently the decay width of the mediator scales like the squared coupling times the mass of the mediator. As long as the mediator is narrow, $\Gamma^2 \ll M^2$[2], increasing M for fixed Λ implies that the couplings grow proportional to M, see eqs.(3.43) and (3.35). In that case the mediator's width will scale like M^3. This means that the $M^2\Gamma^2$ term in the squared propagator of the mediator, as obtained from eqs.(6.2) and (6.1), will scale like M^8 with increasing mass. When the mediator's width becomes comparable to its mass a perturbative treatment is no longer possible; moreover, eqs.(3.43) and (3.35), which ignore the $\Gamma^2 M^2$ term in the squared propagator, are no longer valid.

In order to illustrate this problem, consider the axial-vector case with $M_A = 10\,\mathrm{TeV}$, $\Lambda_{AV} = 1\,\mathrm{TeV}$ and $g_{\chi A} = g_{qA}$ for all six quark flavours. Eq.(3.43) then gives $g_{\chi A} = g_{qA} = \sqrt{10}$, which via eq.(6.1) leads to $\Gamma_A \simeq 50\,\mathrm{TeV} = 5M_A$! This is clearly beyond the domain of perturbation theory, and also beyond the domain of applicability of eq.(3.43).

In our earlier analyses we chose $M_A = 10\,\mathrm{TeV}$ just to be on the safe side; for such a heavy mediator on–shell production of the mediator should clearly be negligible, and the

---

[2] Here, M stands for the mass of the mediator in general. Remember that we add subscripts A and P for specific mediators when required.

EFT limit should be applicable to analyses of LHC data. We saw above that for fixed Λ the mediator's width grows like the third power of its mass. It is thus important to find the *minimal* mass of the mediator for which the predictions of the simplified model can be reproduced accurately by the EFT.

In order to determine this we again only consider contributions with $N_{NP} = 2$. We compute the mono-jet cross-section after cuts for two values of the width of the mediator, $\Gamma = 1\,\text{GeV}$ and $\Gamma = M/2$. In case of an axial-vector mediator, contributions with initial b or t quarks are very small, due to their small parton densities in the proton. For pseudo-scalar mediator, eq.(3.35) implies $g = g_{\chi P} \simeq 62$ for $\Lambda = 40\,\text{GeV}$ (near the current bound) already for $M_P = 1\,\text{TeV}$. Eq.(3.4) would thus imply a coupling g_{Pt} to the top quark well beyond $\sqrt{4\pi}$. For only slightly heavier mediator, its coupling to b quarks would become non-perturbative as well. We, therefore, set the couplings to b and t quarks to zero in both scenarios.

We now compute the cross-section for $\chi\bar{\chi}+$ jet(s) 'mono-jet' events after cuts as a function of the mediator mass, keeping Λ fixed. For $\Gamma = M/2$, we include the width dependence of Γ, i.e. we replace M by $(M^4 + M^2\Gamma^2)^{1/4}$ in eqs.(3.43) and (3.35). We fix Λ_{AV} to 900 GeV and Λ_{PS} to $40\,\text{GeV}$, close to the current experimental limits. Since we only include contributions where a single mediator is exchanged and fix the widths of the mediators, the matrix element is always proportional to the product of couplings of the mediator to quarks and to WIMPs. This is true by construction in the EFT limit but holds here even for on–shell exchange of the mediator.

The results are shown in figs.(6.1). We see that if we fix the mediator's width to $1\,\text{GeV}$, as we did in our previous analyses, it should have a mass of at least $6\,\text{TeV}$ for on–shell production of the mediator to become negligible. Only for masses above this value does the cross-section become independent of the mediator's mass for fixed Λ, as predicted by the EFT. This lower limit is basically the same for axial-vector and pseudo-scalar mediator. These figures use the ATLAS cuts that offer the best-expected sensitivity in the given model; this differs slightly, with the axial-vector model favouring a slightly stronger cut on the $\not{E}_T$.

However, taking such a small width exaggerates the problem. Since the width in this calculation is kept fixed, independent of the mass and couplings of the mediator, the cross-section for on–shell production of the mediator scales like $1/\Gamma$ after integrating over the Breit–Wigner peak. An artificially small width, therefore, implies an artificially large on–shell cross-section. On the other hand, figs.(6.1) also show that even for $\Gamma = M/2$, at the border of the perturbatively treatable domain, the cross-section becomes approximately independent of the mass only for $M \geq 3\,\text{TeV}$.

For fixed product $g_A^2 \equiv g_{\chi A} g_{qA}$ the total decay width of the axial-vector mediator is minimized if $g_{qA}^2 = g_A^2/(2\sqrt{3})$, giving

$$\Gamma_{A,\text{min}} = \frac{M_A g_A^2}{\sqrt{3}\pi} = \frac{M_A^3}{\sqrt{3}\pi\Lambda_{AV}^2} \tag{6.3}$$

here we again assumed equal couplings g_{qA} to all first and second generation quarks, and have used eq.(3.43). Requiring $\Gamma_A < 0.5 M_A$ for a weakly–coupled theory, and $M_A > 3\,\text{TeV}$

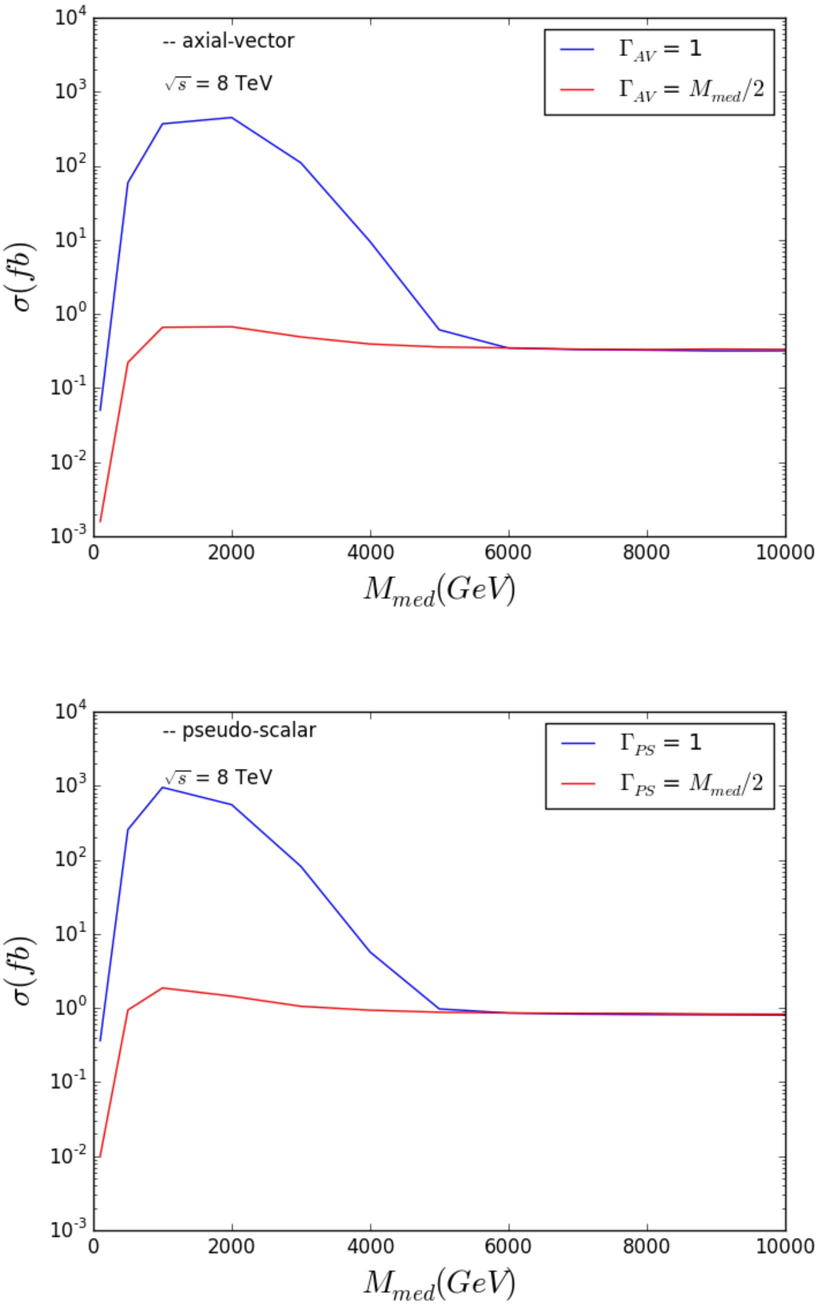

Figure 6.1: Mono-jet cross-section after cuts for two mediator widths. The upper frame is for the axial-vector mediator with $\Lambda_{AV} = 900\,\text{GeV}$ and cuts taken from ATLAS SR7; the bottom frame is for the pseudo-scalar mediator with $\Lambda_{PS} = 40\,\text{GeV}$ and cuts taken from ATLAS SR6. The couplings have been varied along with the mediator masses, such that the scales Λ are kept fixed.

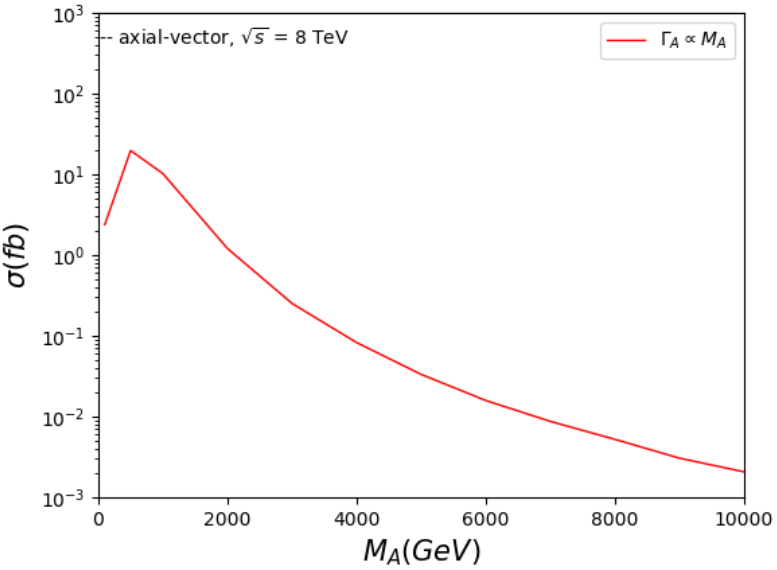

Figure 6.2: Mono-jet cross-section after cuts from ATLAS SR7 in the model with axial-vector mediator if the mediator's width is calculated from eq.(6.1). Here the couplings are varied along with M_A such that Λ_{AV} calculated using eq.(3.43) is kept fixed at 900 GeV.

so that mono-jet production at the 8 TeV LHC can be described adequately by the EFT, thus implies $\Lambda_{AV} > 1.8$ TeV. This is only about a factor of 2 above the lower bound from the 8 TeV data. Recall, however, that the signal cross-section scales like Λ^{-4}; improving the bound by a factor of two would thus require a 16 times stronger upper bound on the signal cross-section! We conclude that for parameter choices that give mono-jet cross-sections near the upper bound, the model with axial-vector mediator *cannot* be accurately described by an EFT, if the theory is weakly coupled, i.e. if perturbation theory is applicable.

This problem can also be illustrated using Fig.(6.2). This shows the mono-jet cross-section after the same cuts, and for the same value of Λ_{AV}, calculated from eq.(3.43). The main difference is that Γ_A has now been computed from eq.(6.1), assuming $g_{\chi A} = g_{qA}$. We see that now there is no region of mediator mass where the cross-section becomes independent of the mass, as one would expect in the EFT picture. The reason is that, as stated above, in this case the width grows like the third power of the mass. For the given choice of couplings, $\Gamma_A > M_A$ for $M_A > 1.5$ TeV. For larger values of M_A, the cross-section drops approximately like M_A^{-4}. Of course, in this regime, the theory is no longer weakly coupled, so the result is not reliable quantitatively. Note also that the situation would have been different had Λ been an order of magnitude larger. In this case, the cross-section would indeed become almost independent of M_A for some range of masses above 3 TeV; it would also be very small, several orders of magnitude below the experimental bound.

We saw in the previous chapters that already the early (2015) 13 TeV data slightly strengthened the bound on Λ_{AV}. However, going to higher center–of–mass energy also requires higher values of M_A for on–shell production of the mediator to be negligible so that the theory can be approximated by an EFT for LHC purposes. For $M_A > 5\,\text{TeV}$, $\Gamma_A < M_A/2$ is possible only if $\Lambda > 3\,\text{TeV}$. It seems extremely unlikely that the upper bounds on the mono-jet cross-section at the LHC will ever become this strong.

The case of pseudo-scalar mediator is slightly different, although the conclusion will be similar. For the assumed proportionality of the coupling to a given quark to the mass of this quark, the total decay width of the mediator is dominated by decay into c quarks and WIMPs. For fixed product $g_P^2 \equiv g_{\chi P} g$ the total decay width is minimized if $g_{\chi P}^2 = \sqrt{3} m_c g_P^2 / v$, giving

$$\Gamma_{P,\min} = \frac{\sqrt{3} M_P^3 m_c}{4\pi \Lambda_{PS}^3} \,. \tag{6.4}$$

Here we have again assumed that the WIMP is much lighter than the mediator, and used eq.(3.35). We again need $M_P > 3\,\text{TeV}$ for the EFT to be applicable even if $\Gamma_P = M_P/2$, see Fig.(6.1). Using a running charm quark mass $m_c(M_P) = 0.6\,\text{GeV}$, we find that $M_P > 3\,\text{TeV}$ and $\Gamma_P < M_P/2$ requires $\Lambda_{PS} > 110\,\text{GeV}$. Recall that in this case the cross-section scales like Λ_{PS}^{-6}. Increasing the lower bound on Λ_{PS} from about 40 to 110 GeV would thus require a reduction of the upper bound on the cross-section by a factor of more than 400. As in case of the axial-vector mediator, the situation is not likely to improve very much at the 13 TeV LHC.

Although we did not treat them explicitly, the cases with vector and scalar $s-$channel mediators are very similar to those with axial-vector and pseudo-scalar mediator, as far as LHC physics is concerned (although the direct detection limits are much stronger for these cases, as noted earlier). We are thus forced to conclude that there is no weakly coupled simplified model with $s-$channel mediator to which the mono-jet bounds derived in the EFT can be applied.

6.3 Implications of the EFT inconsistency

We briefly mention the effects of the $N_{NP} = 4$ contributions to the EFT limits on Λ in the context of our simplified models. For our models described in earlier sections, we determine the limit at which the EFT analysis with double-mediator exchange breaks down, fig.(6.3). For $N_{NP} = 4$, the limits are comparatively stronger and the breakdown of our perturbative theory occurs if mediator mass is $> 6\,\text{TeV}$. Since for our EFT study Λ is proportional to the product of the mediator's couplings to q and χ, in its simplified counterpart, the width has terms $\propto {g_q}^2$ and $\propto {g_\chi}^2$[3]. Also, here we have taken the that $g_q = g_\chi$.

At $\sqrt{s} = 13\,\text{TeV}$ (fig.(6.4)), the cross-sections are significantly larger than the 8 TeV. Here, the break-down limit easily reaches 9 TeV for $N_{NP} = 2$. From the results it is clear

---

[3] Here we drop the subscripts A and P from the couplings in order to make general comments for both the axial-vector and pseudo-scalar cases

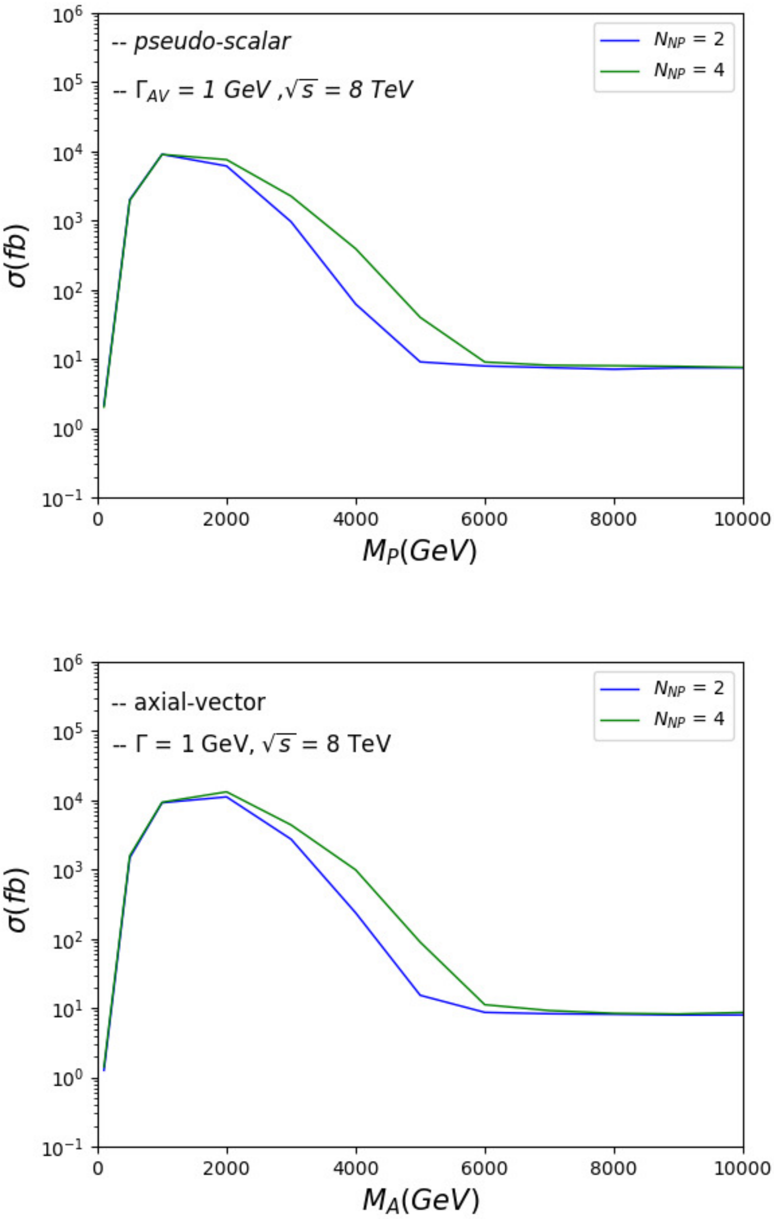

Figure 6.3: Comparison of mono-jet cross-sections for axial-vector and pseudo-scalar models for calculated mediator widths at 8 TeV, for $N_{NP} = 2$ and $N_{NP} = 4$ processes. Note, that $\Gamma = 1\,\text{GeV}$ here for both the axial-vector and pseudo-scalar mediators.

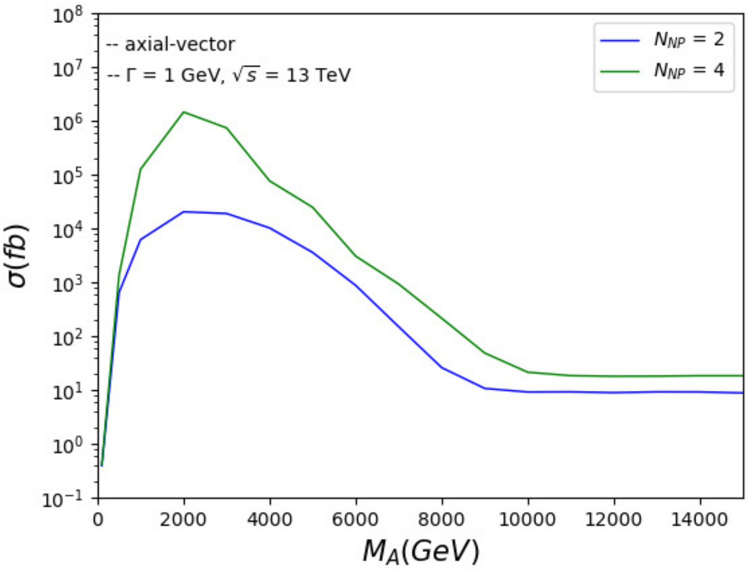

Figure 6.4: Mono-jet cross-section after cuts from ATLAS SR7 in the model with axial-vector mediator if the mediator's width is calculated from eq.(6.1). Here the couplings are varied along with M_A such that Λ_{AV} calculated using eq.(3.43) is kept fixed at 900 GeV.

that as $N_{NP} = 4$ cross-sections behave similar to those of $N_{NP} = 2$, including them still does not benefit us towards a meaningful EFT description of a simplified model.

CHAPTER 7

Conclusion

In this chapter we summarize the key highlights of this thesis. We briefly discuss the dark matter candidates and current searches. We focussed on the WIMP dark matter searches at the LHC. We started by doing an effective field theory analysis to understand the WIMP interactions with the Standard Model particles. We derived the dimension–6 effective operators from a full-theory Lagrangian. For reasons specified earlier, we considered axial-vector and pseudo-scalar operators. Throughout our analysis we had an off-shell mediator of mass 10 TeV to ensure the validity of our effective approach.

We looked into the mono-jet searches as they are the most interesting and probable probes for WIMPs at the proton-proton colliders. Using the EFT framework for our mono-jet analysis, we derived the upper bounds on the WIMP cross-sections. The most sensitive signal regions for deriving the bounds usually have a missing energy, $E_T^{miss} >$ 400 GeV. We reproduced the current limits on the EFT cut-off scale Λ given by ATLAS and CMS to better than 10%, both at $\sqrt{s} = 8$ and 13 TeV. We then obtained combined limits from both the LHC experiments to reduce any discrepancy in the bounds due to systematical uncertainities. However, from our results we found that combining the 8 TeV data from the ATLAS and CMS only improves the results by less than 1%.

Proceeding with the bounds obtained using EFT, we derived a simplified model for WIMPs. We showed that there is no weakly coupled simplified model with $s-$channel axial-vector mediator that can be accurately described by an EFT, as far as the LHC mono-jet analyses are concerned. Our condition for weak coupling was the requirement that the width of the mediator (Γ) is less than half of its mass. In this case, for the on–shell production of the mediator to be negligible, the mediator must have masses much larger than the cut-off scale Λ of the EFT. For this condition to satisfy, the couplings are required to be extremely large which further leads to large decay widths. We demonstrate that complications arise when we formulate a simplified model based on our EFT analyses. For the pseudo-scalar mediator this problem is more severe as a weakly coupled theory is much difficult to obtain. As our couplings to the pseudo-scalar mediator are mass dependent, we observed that the couplings blow up even when we neglect the heavy quarks (bottom and top) in the interactions.

Furthermore, we showed that for the EFT limit, the usual analysis with only single mediator exchange ($N_{NP} = 2$ in the language of MadGraph) underestimates the contributions of some physically inevitable sub-processes. For our mono-jet analysis, we include these sub-processes with a double mediator exchange ($N_{NP} = 4$) at the tree-level. We showed that their contributions to the final signals are of factor greater than two even if only generator–level cuts are imposed. These contributions are even larger for the signal regions after the final cuts are applied, thus resulting in stronger limits on Λ with more than 5% increase. These effects are further enhanced at higher collision energies, for example, the increase in the limits at 13 TeV correspond to an increase in the total cross-section by at least 60%. Our results emphasize that these contributions to the matrix element of the signal process, that scale like Λ^{-4}, are indeed important for a true EFT limit. Thus, for obtaining consistent EFT limits it is important to include all the relevant operators with mass dimension up to eight. As these contributions from sub-processes and higher dimension operators are always present in a physical scenario, it is advised to not ignore them. Such an EFT, however, will have many more parameters than a typical simplified model given the complexities of the higher dimension operators.

Thus, we finally conclude that the model independent approach of using effective field theory analysis for the mono-jet searches, does not apply to any model.

Bibliography

[1] J.-P. Uzan, “The big-bang theory: construction, evolution and status”, 2016, arXiv: `1606.06112 [astro-ph.CO]`, URL: `https://inspirehep.net/record/1471251/files/arXiv:1606.06112.pdf` (cit. on p. 1).

[2] Jeans, J.H., *The Motions of Stars in a Kapteyn Universe*, mnras **82** (1922) 122 (cit. on p. 1).

[3] Oort, J.H., *The force exerted by the stellar system in the direction perpendicular to the galactic plane and some related problems*, bain **6** (1932) 249 (cit. on p. 1).

[4] G. ALTARELLI, *The Standard model of particle physics*, (2005), arXiv: `hep-ph/0510281 [hep-ph]` (cit. on p. 1).

[5] P. A. R. Ade et al., *Planck 2015 results. XIII. Cosmological parameters*, Astron. Astrophys. **594** (2016) A13, arXiv: `1502.01589 [astro-ph.CO]` (cit. on pp. 2, 5, 6).

[6] S. P. Martin, *A Supersymmetry primer*, (1997), [Adv. Ser. Direct. High Energy Phys.18,1(1998)], arXiv: `hep-ph/9709356 [hep-ph]` (cit. on p. 2).

[7] H. P. Nilles, *Supersymmetry: The Final Countdown*, AIP Conf. Proc. **1078** (2009) 3, arXiv: `0809.4390 [hep-th]` (cit. on p. 2).

[8] I. J. R. Aitchison, *Supersymmetry and the MSSM: An Elementary introduction*, (2005), arXiv: `hep-ph/0505105 [hep-ph]` (cit. on p. 2).

[9] C. P. Burgess, *Introduction to Effective Field Theory*, Ann. Rev. Nucl. Part. Sci. **57** (2007) 329, arXiv: `hep-th/0701053 [hep-th]` (cit. on p. 2).

[10] Y. Bai, P. J. Fox and R. Harnik, *The Tevatron at the Frontier of Dark Matter Direct Detection*, JHEP **12** (2010) 048, arXiv: `1005.3797 [hep-ph]` (cit. on pp. 2, 13, 15, 21).

[11] M. Beltran et al., *Maverick dark matter at colliders*, JHEP **09** (2010) 037, arXiv: `1002.4137 [hep-ph]` (cit. on pp. 2, 21).

[12] V. Khachatryan et al., *Search for dark matter, extra dimensions, and unparticles in monojet events in proton–proton collisions at* $\sqrt{s} = 8$ *TeV*, Eur. Phys. J. **C75**.5 (2015) 235, arXiv: `1408.3583 [hep-ex]` (cit. on pp. 2, 9, 24, 30).

[13] G. Aad et al.,
Search for new phenomena in final states with an energetic jet and large missing transverse momentum in pp collisions at $\sqrt{s}$ *=8 TeV with the ATLAS detector*, Eur. Phys. J. **C75**.7 (2015) 299, [Erratum: Eur. Phys. J.C75,no.9,408(2015)], arXiv: `1502.01518 [hep-ex]` (cit. on pp. 2, 9, 15, 24, 25, 30).

[14] M. Papucci, A. Vichi and K. M. Zurek,
Monojet versus the rest of the world I: t-channel models, JHEP **11** (2014) 024, arXiv: `1402.2285 [hep-ph]` (cit. on p. 2).

[15] G. Hinshaw et al., *Nine-Year Wilkinson Microwave Anisotropy Probe (WMAP) Observations: Cosmological Parameter Results*, Astrophys. J. Suppl. **208** (2013) 19, arXiv: `1212.5226 [astro-ph.CO]` (cit. on p. 5).

[16] G. R. Blumenthal et al.,
Formation of Galaxies and Large Scale Structure with Cold Dark Matter, Nature **311** (1984) 517 (cit. on p. 5).

[17] P. A. R. Ade et al., *Planck 2013 results. XVI. Cosmological parameters*, Astron. Astrophys. **571** (2014) A16, arXiv: `1303.5076 [astro-ph.CO]` (cit. on p. 5).

[18] G. Steigman, B. Dasgupta and J. F. Beacom, *Precise Relic WIMP Abundance and its Impact on Searches for Dark Matter Annihilation*, Phys. Rev. **D86** (2012) 023506, arXiv: `1204.3622 [hep-ph]` (cit. on p. 5).

[19] G. Bertone, D. Hooper and J. Silk,
Particle dark matter: Evidence, candidates and constraints, Phys. Rept. **405** (2005) 279, arXiv: `hep-ph/0404175 [hep-ph]` (cit. on p. 6).

[20] K. Freese, *Status of Dark Matter in the Universe*, Int. J. Mod. Phys. **D26**.06 (2017) 1730012, arXiv: `1701.01840 [astro-ph.CO]` (cit. on p. 6).

[21] Zwicky, F., *Republication of: The redshift of extragalactic nebulae*, General Relativity and Gravitation **41** (2009) 207 (cit. on p. 6).

[22] S. Noll et al., *Analysis of galaxy spectral energy distributions from far-UV to far-IR with CIGALE: studying a SINGS test sample*, AandA **507**.3 (2009) 1793, URL: `https://doi.org/10.1051/0004-6361/200912497` (cit. on p. 6).

[23] D. Clowe, S. W. Randall and M. Markevitch,
Catching a bullet: Direct evidence for the existence of dark matter, Nucl. Phys. Proc. Suppl. **173** (2007) 28, arXiv: `astro-ph/0611496 [astro-ph]` (cit. on p. 6).

[24] B. A. Bassett and R. Hlozek, *Baryon Acoustic Oscillations*, (2009), arXiv: `0910.5224 [astro-ph.CO]` (cit. on p. 6).

[25] É. Aubourg et al.,
Cosmological implications of baryon acoustic oscillation measurements, Phys. Rev. **D92**.12 (2015) 123516, arXiv: `1411.1074 [astro-ph.CO]` (cit. on p. 6).

[26] R. Scarpa, *Modified newtonian dynamics, an introductory review*, AIP Conf. Proc. **822** (2006) 253, [,253(2006)], arXiv: `astro-ph/0601478 [astro-ph]` (cit. on p. 6).

[27] J. Abdallah et al., *Simplified Models for Dark Matter and Missing Energy Searches at the LHC*, (2014), arXiv: `1409.2893 [hep-ph]` (cit. on pp. 6, 39).

[28] M. G. e. a. Aartsen, *Searches for Sterile Neutrinos with the IceCube Detector*, Phys. Rev. Lett. **117** (7 2016) 071801, URL: `https://link.aps.org/doi/10.1103/PhysRevLett.117.071801` (cit. on p. 6).

[29] J. Lesgourgues and S. Pastor, *Neutrino mass from Cosmology*, Adv. High Energy Phys. **2012** (2012) 608515, arXiv: `1212.6154 [hep-ph]` (cit. on p. 6).

[30] A. Ringwald, *Alternative dark matter candidates: Axions*, PoS **NOW2016** (2016) 081, arXiv: `1612.08933 [hep-ph]` (cit. on p. 6).

[31] A. Kusenko and M. E. Shaposhnikov, *Supersymmetric Q balls as dark matter*, Phys. Lett. **B418** (1998) 46, arXiv: `hep-ph/9709492 [hep-ph]` (cit. on p. 7).

[32] E. W. Kolb, D. J. H. Chung and A. Riotto, “WIMPzillas!”, *Trends in theoretical physics II. Proceedings, 2nd La Plata Meeting, Buenos Aires, Argentina, November 29-December 4, 1998*, [,91(1998)], 1998 91, arXiv: `hep-ph/9810361 [hep-ph]`, URL: `http://lss.fnal.gov/cgi-bin/find_paper.pl?conf-98-325` (cit. on p. 7).

[33] R. Catena and L. Covi, *SUSY dark matter(s)*, Eur. Phys. J. **C74** (2014) 2703, arXiv: `1310.4776 [hep-ph]` (cit. on p. 7).

[34] H.-C. Cheng, J. L. Feng and K. T. Matchev, *Kaluza-Klein dark matter*, Phys. Rev. Lett. **89** (2002) 211301, arXiv: `hep-ph/0207125 [hep-ph]` (cit. on p. 7).

[35] M. Drees and G. Gerbier, *PDG dark matter review*, Particle Data Group, Chin. Phys. C, 40, 100001 (2016) (2016), eprint: `http://www-pdg.lbl.gov/2016/reviews/rpp2016-rev-dark-matter.pdf` (cit. on p. 7).

[36] T. Saab, “An Introduction to Dark Matter Direct Detection Searches & Techniques”, *The Dark Secrets of the Terascale: Proceedings, TASI 2011, Boulder, Colorado, USA, Jun 6 - Jul 11, 2011*, 2013 711, arXiv: `1203.2566 [physics.ins-det]`, URL: `https://inspirehep.net/record/1093524/files/arXiv:1203.2566.pdf` (cit. on p. 8).

[37] R. Bernabei et al., *Particle Dark Matter in DAMA/LIBRA*, (2010), arXiv: `1007.0595 [astro-ph.CO]` (cit. on p. 8).

[38] T. Marrodán Undagoitia and L. Rauch, *Dark matter direct-detection experiments*, J. Phys. **G43**.1 (2016) 013001, arXiv: `1509.08767 [physics.ins-det]` (cit. on p. 8).

[39] E. Charles et al., *Sensitivity Projections for Dark Matter Searches with the Fermi Large Area Telescope*, Phys. Rept. **636** (2016) 1, arXiv: `1605.02016 [astro-ph.HE]` (cit. on p. 9).

[40] M. G. Aartsen et al., *Search for dark matter annihilations in the Sun with the 79-string IceCube detector*, Phys. Rev. Lett. **110**.13 (2013) 131302, arXiv: `1212.4097 [astro-ph.HE]` (cit. on p. 9).

[41] E. Métral, *LHC: status, prospects and future challenges*, PoS **LHCP2016** (2016) 002 (cit. on p. 9).

[42] J. Abdallah et al., *Simplified Models for Dark Matter Searches at the LHC*, Phys. Dark Univ. **9-10** (2015) 8, arXiv: `1506.03116 [hep-ph]` (cit. on p. 11).

[43] D. Goncalves, P. A. N. Machado and J. M. No, *Simplified Models for Dark Matter Face their Consistent Completions*, Phys. Rev. **D95**.5 (2017) 055027, arXiv: `1611.04593 [hep-ph]` (cit. on p. 12).

[44] A. Pich, "Effective field theory: Course", *Probing the standard model of particle interactions. Proceedings, Summer School in Theoretical Physics, NATO Advanced Study Institute, 68th session, Les Houches, France, July 28-September 5, 1997. Pt. 1, 2*, 1998 949, arXiv: `hep-ph/9806303 [hep-ph]` (cit. on p. 12).

[45] B. Gripaios, *Lectures on Effective Field Theory*, (2015), arXiv: `1506.05039 [hep-ph]` (cit. on p. 12).

[46] A. V. Manohar, *Effective field theories*, Lect. Notes Phys. **479** (1997) 311, arXiv: `hep-ph/9606222 [hep-ph]` (cit. on p. 12).

[47] K. Cheung et al., *Global Constraints on Effective Dark Matter Interactions: Relic Density, Direct Detection, Indirect Detection, and Collider*, JCAP **1205** (2012) 001, arXiv: `1201.3402 [hep-ph]` (cit. on p. 12).

[48] A. De Simone et al., *On the effective operators for Dark Matter annihilations*, JCAP **1302** (2013) 039, arXiv: `1301.1486 [hep-ph]` (cit. on p. 12).

[49] A. Belyaev et al., *Dark Matter characterization at the LHC in the Effective Field Theory approach*, JHEP **04** (2017) 110, arXiv: `1610.07545 [hep-ph]` (cit. on p. 12).

[50] D. Schmeier, *Effective Models for Dark Matter at the International Linear Collider*, PhD thesis: Bonn U., 2013, arXiv: `1308.4409 [hep-ph]`, URL: `https://inspirehep.net/record/1250012/files/arXiv:1308.4409.pdf` (cit. on p. 12).

[51] J. Fan, M. Reece and L.-T. Wang, *Non-relativistic effective theory of dark matter direct detection*, JCAP **1011** (2010) 042, arXiv: `1008.1591 [hep-ph]` (cit. on p. 13).

[52] W. Altmannshofer et al.,
Dark Matter Signals in Dilepton Production at Hadron Colliders,
Phys. Rev. **D91**.11 (2015) 115006, arXiv: `1411.6743 [hep-ph]` (cit. on p. 13).

[53] A. Berlin, T. Lin and L.-T. Wang,
Mono-Higgs Detection of Dark Matter at the LHC, JHEP **06** (2014) 078,
arXiv: `1402.7074 [hep-ph]` (cit. on p. 14).

[54] C. Csaki, *The Minimal supersymmetric standard model (MSSM)*,
Mod. Phys. Lett. **A11** (1996) 599, arXiv: `hep-ph/9606414 [hep-ph]`
(cit. on p. 14).

[55] N. F. Bell et al.,
W/Z Bremsstrahlung as the Dominant Annihilation Channel for Dark Matter,
Phys. Rev. **D83** (2011) 013001, arXiv: `1009.2584 [hep-ph]` (cit. on p. 14).

[56] M. Peskin and D. Schroeder, *An Introduction To Quantum Field Theory*,
Frontiers in Physics, Avalon Publishing, 1995, ISBN: 9780813345437,
URL: `https://books.google.de/books?id=EVeNNcslvX0C` (cit. on pp. 15, 57).

[57] T. C. Collaboration, *The CMS experiment at the CERN LHC*,
Journal of Instrumentation **3**.08 (2008) S08004,
URL: `http://stacks.iop.org/1748-0221/3/i=08/a=S08004` (cit. on p. 22).

[58] T. A. Collaboration, *The ATLAS Experiment at the CERN Large Hadron Collider*,
Journal of Instrumentation **3**.08 (2008) S08003,
URL: `http://stacks.iop.org/1748-0221/3/i=08/a=S08003` (cit. on p. 22).

[59] A. Alloul et al., *FeynRules 2.0 - A complete toolbox for tree-level phenomenology*,
Comput. Phys. Commun. **185** (2014) 2250, arXiv: `1310.1921 [hep-ph]`
(cit. on p. 23).

[60] C. Degrande et al., *UFO - The Universal FeynRules Output*,
Comput. Phys. Commun. **183** (2012) 1201, arXiv: `1108.2040 [hep-ph]`
(cit. on p. 23).

[61] J. Alwall et al., *The automated computation of tree-level and next-to-leading order differential cross sections, and their matching to parton shower simulations*,
JHEP **07** (2014) 079, arXiv: `1405.0301 [hep-ph]` (cit. on p. 23).

[62] A. Buckley et al., *General-purpose event generators for LHC physics*,
Phys. Rept. **504** (2011) 145, arXiv: `1101.2599 [hep-ph]` (cit. on p. 23).

[63] M. H. Seymour, “Monte Carlo for the LHC”, *Physics at the LHC2010. Proceedings, 5th Conference, PLHC2010, Hamburg, Germany, June 7-12, 2010*, 2010 147,
arXiv: `1008.2927 [hep-ph]`,
URL: `https://inspirehep.net/record/865463/files/arXiv:1008.2927.pdf`
(cit. on p. 23).

[64] A. D. Martin et al., *Parton distributions for the LHC*,
Eur. Phys. J. **C63** (2009) 189, arXiv: `0901.0002 [hep-ph]` (cit. on p. 23).

[65] J. R. Andersen et al., *Les Houches 2013: Physics at TeV Colliders: Standard Model Working Group Report*, - (2014), arXiv: `1405.1067 [hep-ph]` (cit. on p. 23).

[66] T. Sjostrand, S. Mrenna and P. Z. Skands, *PYTHIA 6.4 Physics and Manual*, JHEP **05** (2006) 026, arXiv: `hep-ph/0603175 [hep-ph]` (cit. on p. 24).

[67] J. Alwall et al., *Comparative study of various algorithms for the merging of parton showers and matrix elements in hadronic collisions*, Eur. Phys. J. **C53** (2008) 473, arXiv: `0706.2569 [hep-ph]` (cit. on p. 24).

[68] M. Drees et al., *CheckMATE: Confronting your Favourite New Physics Model with LHC Data*, Comput. Phys. Commun. **187** (2015) 227, arXiv: `1312.2591 [hep-ph]` (cit. on p. 24).

[69] D. Dercks et al., *CheckMATE 2: From the model to the limit*, - (2016), arXiv: `1611.09856 [hep-ph]` (cit. on p. 24).

[70] J. de Favereau et al., *DELPHES 3, A modular framework for fast simulation of a generic collider experiment*, JHEP **02** (2014) 057, arXiv: `1307.6346 [hep-ex]` (cit. on p. 24).

[71] M. Cacciari, G. P. Salam and G. Soyez, *FastJet User Manual*, Eur. Phys. J. **C72** (2012) 1896, arXiv: `1111.6097 [hep-ph]` (cit. on p. 24).

[72] J. S. Kim et al., *A framework to create customised LHC analyses within CheckMATE*, Comput. Phys. Commun. **196** (2015) 535, arXiv: `1503.01123 [hep-ph]` (cit. on p. 24).

[73] T. Junk, *Confidence level computation for combining searches with small statistics*, Nucl. Instrum. Meth. **A434** (1999) 435, arXiv: `hep-ex/9902006 [hep-ex]` (cit. on pp. 24, 30).

[74] M. Cacciari, G. P. Salam and G. Soyez, *The Anti-k(t) jet clustering algorithm*, JHEP **04** (2008) 063, arXiv: `0802.1189 [hep-ph]` (cit. on p. 24).

[75] M. Aaboud et al., *Search for new phenomena in final states with an energetic jet and large missing transverse momentum in pp collisions at* $\sqrt{s}$ *=13 TeV with the ATLAS detector*, Phys. Rev. **D94**.3 (2016) 032005, arXiv: `1604.07773 [hep-ex]` (cit. on p. 26).

[76] L. Lista, "Practical Statistics for Particle Physicists", *2016 European School of High-Energy Physics (ESHEP 2016) Skeikampen, Norway, June 15-28, 2016*, 2016, arXiv: `1609.04150 [physics.data-an]`, URL: `https://inspirehep.net/record/1486520/files/arXiv:1609.04150.pdf` (cit. on p. 30).

[77] P. Harris et al., *Constraining Dark Sectors at Colliders: Beyond the Effective Theory Approach*, Phys. Rev. **D91** (2015) 055009, arXiv: `1411.0535 [hep-ph]` (cit. on p. 39).

[78] M. R. Buckley, D. Feld and D. Goncalves,
Scalar Simplified Models for Dark Matter, Phys. Rev. **D91** (2015) 015017,
arXiv: `1410.6497 [hep-ph]` (cit. on p. 39).

APPENDIX A

Appendix

A.1 Decay width of axial-vector mediator

We calculate the decay width of an axial-vector mediator within a simplified model, using [56].

The probability of transition of a particle from initial state $\mid i >$ to final state $\mid f >$ is proportional to the S-matrix

$$P_{i \to f} \propto S_{fi} \tag{A.1}$$

where, $S_{fi} = (2\pi)^4 \delta^4(p_f - p_i) M_{fi}$ is the S-matrix - the limiting unitary operator defining the particle states at any common reference time. M_{fi} is the reduced matrix element, and p_i and p_f are momenta of initial and final states, respectively.

For a collision of particles A and B resulting in multiple final states, such that particle states $A\ B \to$ 1,2,3...n, the probability of this transition can be given as:

$$P_{(AB \to 1,2,..,n)} = \prod_f \frac{d^3 p_f}{(2\pi)^3} \frac{1}{2E_f} |\langle p_1 ... p_n | \phi_A \phi_B \rangle_{in}|^2 \tag{A.2}$$

Here,E_f is the total energy of the final states. ϕ_A and ϕ_B correspond to the initial states of respective particles. On describing the initial and final states in terms of the initial state momenta (k_A and k_B) and the final state momenta, p_f for $f = 1, 2, 3...n$, one can get the complete transition as:

$$\langle p_1 p_2 ... | iT | k_A k_B \rangle = (2\pi)^4 \delta^4 \left(k_A + k_B - \sum p_f \right) i\mathcal{M} \left(k_A, k_B \to \{p_f\} \right) \tag{A.3}$$

Here, $M(k_A, k_B \to \{p_f\})$ is the invariant matrix element. Here, all of the the four momenta ($p^0 = E_p, k^0 = E_k$) involved in the transition are on mass-shell. Thus the cross-section can be given as:

$$d\sigma = \frac{1}{2E_A 2E_B |v_A - v_B|} \left(\prod_f \frac{d^3 p_f}{(2\pi)^3} \frac{1}{2E_f} \right) |\mathcal{M}(p_A, p_B \to \{p_f\})|^2 (2\pi)^4 \delta^4 \left(p_A + p_B - \sum p_f \right) \tag{A.4}$$

Integrating over the final state momenta:

$$\int d\prod_n = \left(\prod_f \int \frac{d^3 p_f}{(2\pi)^3} \frac{1}{2E_f} \right) (2\pi)^4 \delta^4 \left(p - \sum p_f \right) \tag{A.5}$$

where, P is the total initial momentum.

$$\frac{1}{E_A E_B |v_A - v_B|} = \frac{1}{E_B {p_A}^2 - E_A {p_B}^2} = \frac{1}{\sum_{\mu\nu} p^\mu p^\nu} \tag{A.6}$$

Thus, the differential cross-section in center of mass frame (total energy of the system is E_{cm}), for two initial state particles going to two particles in final state is given by:

$$\left(\frac{d\sigma}{d\Omega} \right)_{cm} = \frac{1}{2E_A 2E_B |v_A - v_B|} \frac{|p_1|}{(2\pi)^2 4E_{cm}} |\mathcal{M}\left(p_A p_B \to p_1 p_2 \right)|^2 \tag{A.7}$$

Now, in order to make this expression valid of our which in our case the axial-vector mediator (A), we neglect all the terms coming from second initial state. Also, as our particle is relatively heavy and decays, it is considered to be at rest in the center of mass frame. Thus, the partial width for of the mediator to its decay components is given as:

$$d\Gamma = \frac{1}{2M_A} \left(\prod_f \frac{d^3 p_f}{(2\pi)^3} \frac{1}{2E_f} \right) |\mathcal{M}(M_A \to \{P_f\})|^2 (2\pi)^4 \delta^4 \left(p_A - \sum p_f \right) \tag{A.8}$$

Thus, the total decay width for the mediator can then be given as:

$$\Gamma = \int d\Gamma = \frac{1}{2M_A} \int \prod_f \frac{d^3 p_f}{(2\pi)^3} \frac{1}{2E_f} |\mathcal{M}(m_A \to \{p_F\})|^2 (2\pi)^4 \delta^4 \left(p_A - \sum p_f \right) \tag{A.9}$$

$$\Gamma = \frac{1}{2M_A} |\mathcal{M}(M_A \to \{p_f\})|^2 \prod_f \int \frac{d^3 p_f}{(2\pi)^3} \frac{1}{2E_f} (2\pi)^4 \delta^4 \left(p_A - \sum p_f \right) \tag{A.10}$$

For two particles (1,2) in the final state, we have:

$$\int d\prod_2 = \int \frac{dp_1 {p_1}^2 d\Omega}{(2\pi)^3 2E_1 2E_2} 2\pi \delta \left(E_{cm} - E_1 - E_2 \right) \tag{A.11}$$

where, $E_1 = \sqrt{p_1^2 + m_1^2}$ and $E_2 = \sqrt{p_2^2 + m_2^2}$ with m_1 and m_2 being their masses, and Ω

is the solid angle in the phase-space.

$$\int d\prod_2 = \int d\Omega \frac{p_1^2 d\Omega}{(2\pi)^3 2E_1 2E_2}\left(\frac{P_1}{E_1} + \frac{P_1}{E_2}\right)^{-1} = \int d\Omega \frac{1}{16\pi^2}\frac{|P_1|}{E_{cm}} \tag{A.12}$$

For symmetric reactions about the collision axis, we can write Ω in terms of the polar angle θ. Thus, the two body phase space equation will become:

$$\int d\prod_2 = \int d\cos\theta \frac{1}{16\pi}\frac{2|p_1|}{E_{cm}} \tag{A.13}$$

At very high energies, $E_{cm} \equiv 1$. Thus, the total width for the axial-vector mediator will become:

$$\Gamma = \frac{1}{2M_A}\frac{|p_1|}{(2\pi)^2 4E_{cm}}|\mathcal{M}(M_A \to \{p_f\}|^2 \tag{A.14}$$

A.1.1 Matrix element for axial-vector mediator

Here, we have the final states being same particles (say for now, WIMP χ) with same mass (m) but different wave functions. The matrix element then for the interaction vertex of the mediator with decay components is be given as

$$-iM_{fi} = \bar{u}(p_1)\left(-ig_\chi \gamma_\mu \gamma^5\right) v(p_2)\epsilon^\nu \tag{A.15}$$

$\therefore$

$$|\mathcal{M}|^2 = \frac{1}{3}\sum_s \sum |\mathcal{M}|^2 \tag{A.16}$$

Taking the product for matrix element and expanding, we get:

$$|\mathcal{M}|^2 = \frac{1}{3}{g_\chi}^2 \sum \left(\bar{v}(p_2)(\gamma^\mu \gamma^5 u(p_1)\right)(\bar{u}(p_1)(\gamma_\mu \gamma_5 v(p_2)) \tag{A.17}$$

$$|\mathcal{M}|^2 = \frac{1}{3}{g_\chi}^2 \bar{v}(p_2)v(p_2)\gamma_\mu\gamma_5\bar{u}(p_1)u(p_1) \tag{A.18}$$

The wave functions above are $\bar{v}(p_2)v(p_2) = \not{p}_2 + m$ and $\bar{u}(p_1)u(p_1) = \not{p}_1 - m$. $\therefore$

$$|\mathcal{M}|^2 = \frac{1}{3}g_\chi^2 \left(\not{p}_2 + m\right)\gamma_\mu\gamma_5(\not{p}_1 - m)\sum \epsilon^\mu {\epsilon_\nu}^* \tag{A.19}$$

$$|\mathcal{M}|^2 = \frac{1}{3}g_\chi^2 \left[tr\left(\not{p}_2 + m\right)\gamma_\mu\gamma_5(\not{p}_1 - m)\right]\sum \epsilon^\mu {\epsilon_\nu}^* \tag{A.20}$$

$$|\mathcal{M}|^2 = \frac{1}{3}g_\chi^2 \left[tr\left(\not{p}_2 + m\right)(\not{p}_1 - m)\right]\sum \epsilon^\mu {\epsilon_\nu}^* \tag{A.21}$$

$$|\mathcal{M}|^2 = \frac{1}{3}g_\chi^2 tr\left(\not{p}_2 \cdot \not{p}_1 - m^2\right) \tag{A.22}$$

$$|\mathcal{M}|^2 = \frac{1}{3}g_\chi^2 8(p_2 \cdot p_1 - m^2) \tag{A.23}$$

$$|\mathcal{M}|^2 = \frac{8}{3}g_\chi^2\left(\frac{M_A^2}{2} - m_\chi^2 - m_\chi^2\right) \tag{A.24}$$

$$|\mathcal{M}|^2 = \frac{8}{3}g_\chi^2\left(\frac{M_A^2}{2} - 2m_\chi^2\right) \tag{A.25}$$

$$|\mathcal{M}|^2 = \frac{4}{3}g_\chi^2 M_A^2\left(1 - \frac{4m_\chi^2}{m_A^2}\right) \tag{A.26}$$

A.1.2 Calculation of phase-space factor

$$\delta^4\left(p_A - (p_2 + p_1)\right) = \frac{E}{2|p|}\delta\left(|p| - \frac{M_A}{2}\sqrt{1 - \frac{4m_\chi^2}{M_A^2}}\right)\delta^3(p_2 + p_1) \tag{A.27}$$

$\therefore$

$$\int d\prod_2 = \int \frac{d^3p}{(2\pi)^3}\frac{d^3p}{(2\pi)^3}\frac{(2\pi)^4}{(2\pi)^3}\frac{(2\pi)^4}{4E^2}\frac{E}{|p|}\left(|p| - \sqrt{\frac{M_A^2}{4} - m^2}\right)\delta^3(p_2 + p_1) \tag{A.28}$$

$$\int d\prod_2 = \frac{1}{32\pi^2}\int d^3p \frac{1}{E|p|}\delta\left(|p| - \sqrt{\frac{M_A^2}{4} - m^2}\right) \tag{A.29}$$

$$\int d\prod_2 = \frac{1}{32\pi^2}\int_0^{4\pi} d\Omega \int_0^{\infty} d|p| \left(\frac{|p|^2}{E|p|}\right)\delta\left(|p| - \sqrt{\frac{M_A^2}{4} - m^2}\right) \tag{A.30}$$

$$\int d\prod_2 = \frac{1}{8\pi}\int d|p|\delta\left(|p| - \sqrt{\frac{M_A^2}{4} - m^2}\right) \tag{A.31}$$

$$\int d\prod_2 = \frac{1}{8\pi}\frac{\sqrt{\frac{M_A^2}{4} - m^2}}{\sqrt{m^2 + \frac{M_A^2}{4} - m^2}} \tag{A.32}$$

$$\int d\prod_2 = \frac{1}{8\pi}\left(1 - \frac{4m_\chi^2}{M_A^2}\right)^{1/2} \tag{A.33}$$

Thus, by putting together eq.(A.26) and eq.(A.33) in eq.(A.14), the total width for an axial-vector mediator decaying into two dark matter particles is given as:

$$\Gamma = \frac{1}{2M_A}g_\chi^2 M_A^2 \frac{16}{3}\left(1 - \frac{4m_\chi^2}{M_A^2}\right) \cdot \frac{1}{8\pi}\left(1 - \frac{4m_\chi^2}{M_A^2}\right)^{1/2} \tag{A.34}$$

Thus,

$$\Gamma = \frac{M_A}{12\pi}g_\chi^2\left(1 - \frac{4m_\chi^2}{M_A^2}\right)^{3/2} \tag{A.35}$$

Similarly, the decays width of the mediator to a pair of quarks will be:

$$\Gamma = 3\frac{M_A}{12\pi}g_q^2\left(1 - \frac{4m_q^2}{M_A^2}\right)^{3/2} \tag{A.36}$$

Combining these, the total decay width of the mediator in our simplified model can finally be given as:

$$\Gamma = \frac{M_A}{12\pi}g_\chi^2\left(1 - \frac{4m_\chi^2}{M_A^2}\right)^{3/2} + \frac{N_c g_q^2}{12\pi}M_A\sum_q\left(1 - \frac{4m_q^2}{m_A^2}\right)^{3/2} \tag{A.37}$$

here, $N_c = 3$ for all coloured particles.

List of Figures

2.1 The three categories of dark matter searches related to each other with crossing symmetry. Here, DM stands for Dark Matter particles, and SM for Standard Model particles. 8

3.1 An interaction vertex is shown in the middle. The diagram conveys how a WIMP-SM interaction via an axial-vector (A) and a pseudo-scalar (P) mediator in a full theory can be understood as a four point interaction in EFT. 12

4.1 A Feynman diagram representation of a mono-jet event for the four–point EFT interaction vertex corresponding to eq.(4.1). 22
4.2 Our limits on the strength of the axial-vector interaction derived using CheckMATE, compared to the ATLAS limits on Λ_{AV} at 95% C.L. and CMS limits on Λ_{AV} at 90% C.L. for $\sqrt{s} = 8\,\text{TeV}$. 28
4.3 Our limits on Λ_{PS} derived using CheckMATE, compared to the ATLAS limits on scalar interaction at 95% C.L. for $\sqrt{s} = 8\,\text{TeV}$. 29
4.4 Bounds on Λ_{AV} for axial-vector interaction at 95% C.L. compared to the ATLAS data taken in 2015 at $\sqrt{s} = 13\,\text{TeV}$. 29

5.1 EFT interaction with $N_{NP} = 4$ having a double mediator exchange . . . 32
5.2 Comparison of bounds on Λ at 95% C.L. derived from ATLAS (up), and at 90% C.L. derived from CMS data (bottom), at $\sqrt{s} = 8\,\text{TeV}$. The blue curves are for $N_{NP} = 2$, i.e. only diagrams where a single mediator is exchanged are included, while the red curves for $N_{NP} = 4$ also include diagrams where two mediators are exchanged. Also, we have set $g_{\chi A} = g_{qA}$. 33
5.3 Comparison of bounds on Λ at 95% C.L. derived from ATLAS at 13 TeV. Again, here the blue curves are for $N_{NP} = 2$, i.e. only diagrams where a single mediator is exchanged are included, while the red curves also include diagrams where two mediators are exchanged ($N_{NP} = 4$). We have set $g_{\chi A} = g_{qA}$. 34
5.4 Comparison of ATLAS' bounds on Λ_{AV} at 95% C.L. for $N_{NP} = 4$ for different coupling ratios. 35

6.1 Mono-jet cross-section after cuts for two mediator widths. The upper frame is for the axial-vector mediator with $\Lambda_{AV} = 900\,\mathrm{GeV}$ and cuts taken from ATLAS SR7; the bottom frame is for the pseudo-scalar mediator with $\Lambda_{PS} = 40\,\mathrm{GeV}$ and cuts taken from ATLAS SR6. The couplings have been varied along with the mediator masses, such that the scales Λ are kept fixed. 42

6.2 Mono-jet cross-section after cuts from ATLAS SR7 in the model with axial-vector mediator if the mediator's width is calculated from eq.(6.1). Here the couplings are varied along with M_A such that Λ_{AV} calculated using eq.(3.43) is kept fixed at $900\,\mathrm{GeV}$. 43

6.3 Comparison of mono-jet cross-sections for axial-vector and pseudo-scalar models for calculated mediator widths at $8\,\mathrm{TeV}$, for $N_{NP} = 2$ and $N_{NP} = 4$ processes. Note, that $\Gamma = 1\,\mathrm{GeV}$ here for both the axial-vector and pseudo-scalar mediators. 45

6.4 Mono-jet cross-section after cuts from ATLAS SR7 in the model with axial-vector mediator if the mediator's width is calculated from eq.(6.1). Here the couplings are varied along with M_A such that Λ_{AV} calculated using eq.(3.43) is kept fixed at $900\,\mathrm{GeV}$. 46

List of Tables

5.1 Our ATLAS' and CMS' limits on Λ_{AV} for different coupling ratios at $\sqrt{s} = 8\,\mathrm{TeV}$ based on $N_{NP} = 4$ processes. 35